AN ABSTRACT OF THE PROJECT OF

Matthew R. Evans for the degree of Masters of Science in Civil Engineering presented on June 6, 2016

Title: Hydrodynamic Loads on Fiber-Optic Micro Cables

Abstract Approved:

Solomon C. Yim

A Finite Element Model of a deployed Fiber-Optic Micro Cable (FOMC) was performed using the marine cable modeling software, OrcaFlex. The focus of this study was a parametric analysis of a two-part, towed cable array with the FOMC dragged behind a depressor and connected to a drogue chute. Length-to-diameter ratios ranged from 3×10^5 to 2×10^6. Cable diameter was found to be the most critical parameter because of its influence on buoyancy while the tangential drag coefficient was surprisingly unimportant due to the presence of the drogue. Semi-analytical expressions to predict tension and cable elevation are presented as well as recommendations on equipment required to perform a physical experiment. The results were applied to a modified setup of the physical experiment that will deploy the FOMC from a Remotely Operated Vehicle (ROV) to an anchored mooring line. Recommended peel tensions for the tension controlled winch are provided.

Hydrodynamic Loads on Fiber-Optic Micro Cables

by
Matthew R. Evans

A PROJECT

submitted to

Oregon State University

in partial fulfillment of
the requirements for the
degree of

Master of Science

Presented June 6, 2016
Commencement June 2016

Master of Science project of Matthew R. Evans presented on June 6, 2016.

APPROVED:

Major Professor, representing Civil Engineering

Head of the School of Civil and Construction Engineering

I understand that my project will become part of the permanent collection of Oregon State University libraries. My signature below authorizes release of my thesis to any reader upon request.

Matthew R. Evans, Author

ACKNOWLEDGEMENTS

I would like to express sincere appreciation for the support I have received over the last 18 months in pursuit of achieving this momentous goal. First, I would like to thank my advisor, Dr. Solomon Yim, for his time and encouragement in completing this project. Also, my advisors from the Naval Facilities Engineering Command, Engineering and Expeditionary Warfare Center, James Schneider and Ryan Seltzer, trusted that I could contribute to their team. Thank you for giving me the opportunity to work with you and establish a better of understanding of the U.S. Navy's research opportunities and needs. My committee members, Dr. Dan Cox and Dr. Merrick Haller, not only supported this project but were also fantastic contributors to providing a successful course load that met both Oregon State University's and the Navy Graduate Program requirements.

A special thanks is extended to Dr. Annette von Jouanne for providing critical access to her license of OrcaFlex software, and to Junhui Lou who provided hours of training in how to use the program.

I must also thank the U.S. Navy, the Civil Engineer Corps, and the Ocean Facilities Program for providing the financial support for me and my family while pursuing this degree. I look forward to paying them back with years of productive and exciting service to our nation.

And finally, my wonderful wife and best friend, Nicole, who is the rock of our family. She has supported me while we dragged our family to every coast in the continental U.S. and even overseas. She has spent a cumulative year and a half of our ten years of marriage raising our now five children completely on her own during my weeks and months away during my time in the Navy. She seems to do it effortlessly, but I know how hard she works every day to help our little family reach our goals. I love you, Nicole, with all my heart.

It has been a great privilege to study and work alongside experts in the field of Coastal and Ocean Engineering and I look forward to applying this newly gained knowledge in support of the U.S. Navy and the engineering community.

TABLE OF CONTENTS

LIST OF FIGURES

LIST OF TABLES

Hydrodynamic Loads on Fiber-Optic Micro Cables

1. Introduction and Background

The Defense Advanced Research Projects Agency (DARPA) is currently in the initial phase of the Tactical Undersea Network Architectures (TUNA) program that seeks to design, produce, and test a rapidly deployable undersea military data network. The system will be comprised of buoy transfer nodes connected to buoyant fiber-optic micro cables (FOMC) that can last up to thirty days (Versprille, 2016). The phase one, $1.9 million contract was awarded to LGS Innovation in September 2015 with the initial concept based on Linden Photonics, Inc.'s Strong Torpedo Fiber Optic Cable (STFOC) (Figure 1). Commercially available fibers from Linden Photonics range from 0.6 mm to 3.2 mm with tensile strengths ranging from 178 N to 311 N (40 lbs-f to 70 lbs-f) with production lengths above 25 km (Linden Photonics, Inc., 2014). A liquid crystal polymer (LCP) provides increased tensile strength and reduced moisture absorption (Linden Photonics, Inc., 2006).

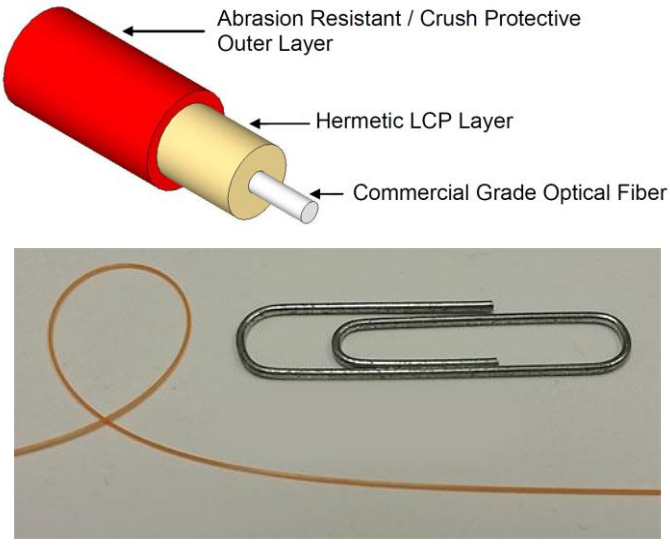

Figure 1. Linden Photonics, Inc.'s Strong Torpedo Fiber Optic Cable (courtesy Linden Photonics & National Defense).

The Naval Facilities Engineering Command, Engineering and Expeditionary Warfare Center (EXWC) is supporting the TUNA project by performing the testing the deployment and durability of the FOMC. The original field test was designed to test the strength and drag characteristics of the cable. A 1 km FOMC was to be towed from a ship at varying velocities to determine the strength and position relationships. The focus of this project provides the parametric analysis via a computer model using the commercial software OrcaFlex prior to support the originally planned field study. On May 12, 2016 the author learned from EXWC that the field study was redesigned to focus more on the deployment feasibility by using a Remotely Operated Vehicle (ROV) to pay out cable attached to a moored buoy line. A general discussion is provided to see how conclusions from the parametric analysis apply to this new setup including providing environmental and prototype test limits based on given peel and brake tensions.

2. Towed Cable Theory

Towed cable arrays in a fluid have been extensively studied since the 1960s with the principle focus on military applications such as towed sonar arrays. Paidoussis (1966, 1973) developed the Paidoussis Equation which provides a linearized equation of motion of a towed flexible cylinder and has provided the basis for nearly all subsequent experiments. Further experimentation and derivation of the non-linear equation of motion of cantilevered flexible strings with a free end demonstrated that string flutter becomes more unstable in longer strings that are sufficiently streamlined but can be controlled by a blunt end (see the series by Paidoussis et al. (2002), Semler et al. (2002), and Lopes et al. (2002) for the nonlinear equations of motion; see further analysis by de Langre et al. (2007), Kheiri et al. (2013)). De Langre et al. (2007) showed that the front-most cable section remains stable because of the tension caused by skin friction, but at some distance from the end, there is no longer enough cable downstream to provide the required amount of tension and the cable begins to oscillate. Previous to de Langre et al. (2007), Trantafyllou and Chryssostomidis (1985) showed analytically

that cables are inherently stable if lacking all rigidity (as determined by a length-to-diameter ratio being less than $1/(2Cd_T)$ where Cd_T is the skin friction coefficient) or if tension is provided at the free end that exceeds $\rho\pi D^2V_o^2/4$, where ρ, D, and V_o are the density of water, the diameter of the cable, and U the free flow velocity, respectively.

Computer algorithms for the dynamic response of cables in a fluid have been widely studied to support cable deployment operations, including estimating the effects of the pre-set peel point tension and rate of cable deployment. A summary of the various Lumped-Parameter, Finite Element Model (FEM), Imaginary Reaction, and Direct Integration algorithms is provided by Leonard and Karnoski (1990). The computer simulations in this project are performed using the FEM software OrcaFlex to estimate forces and responses of the system. OrcaFlex is a "fully three-dimensional non-linear time domain finite element program" used to model forces in the marine environment (Orcina, 2009). It is used principally by the oil and gas and defense industries to analyze wave and drag forces on slender structures. The version used here is 9.3a with modules for Statics and Dynamics.

The governing equation for motion in OrcaFlex is given as:

$$M(p,a) = F(p,v,t) - C(p,v) - K(p) \qquad (1)$$

where M(p,a) is the system inertia load, C(p,v) is the system damping load, K(p) is the system stiffness load, F(p,v,t) is the external load, p,v and a are the position, velocity, and acceleration vectors, respectively, and t is time. The variable t is the simulation time. Damping and stiffness loads are parameters of the object. Cables, for example, are simulated as an array of lump mass elements connected by massless springs, with parameters determined by stiffness and damping coefficients. The equation of motion is solved iteratively with the choice of either an explicit or implicit scheme.

Forces on a floating cable include gravity, buoyancy, inertial forces, drag, and contact forces with other objects or bottom. Of primary importance to computing the cable response is

understanding hydrodynamic drag force and predicting the drag coefficient, Cd. Drag forces are given by:

$$F_x = (1/2)\rho Cd_x A_x V_x|V_x| \quad (2)$$

where F_X is the force, ρ is the density of the water, Cd_X is the drag coefficient, A_X is the drag area, and V_X is the local relative velocity of the fluid. The subscript x denotes the direction of the drag. Based on the independence principle, OrcaFlex splits drag forces between normal and axial drag components (Figure 2). This simplification was shown to be accurate by Choc & Casarella (1971) and is useful as drag components have been thoroughly studied (for axial flow drag studies, see Reid & Wilson (1962), White (1972), Rispin (1977), Holler (1984), and Karnoski (1991)) and are quickly obtainable from design charts such as ESDU 80025 (1986). The drag coefficient is dependent not only on the shape but also the Reynolds number, Re, roughness, ε, and angle of attack, α. Equations for F_N and F_T are provided as equations (3) and (4). OrcaFlex uses a drag area of DL and πDL, respectively, for normal drag and tangential drag. Sources for Cd are discussed later.

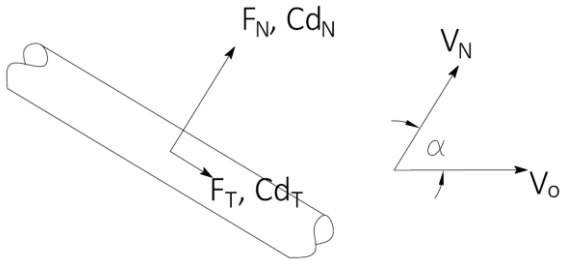

Figure 2. Cable coordinates.

$$F_N = \frac{1}{2}\rho Cd_N(DL)|V_o|V_o \cos^2(\alpha) \quad (3)$$

$$F_T = \frac{1}{2}\rho Cd_T(\pi DL)|V_o|V_o \sin^2(\alpha) \quad (4)$$

Buoyancy of the cylinder is also expected to produce large changes in the final depth of the cable. Vertical forces on the system include the vertical component of tension on the strength member, vertical components of the drag forces, and the wet weight:

$$F_B - F_W = (\gamma_{FO} - 1)\rho g \quad (5)$$

where F_B is the buoyant force, F_W is the dry weight, γ_{FO} is the specific gravity of the cable given as $\gamma_{FO} = \rho_{FO}/\rho$, ρ_{FO} is the density of the cable and ρ is the density of water.

Although not central to this study, but applicable to planning deployment methods of FOMCs, a study by Zhou et al. (2008) looked at the sinkage rate of fiber-optic micro cables from the surface upon initial deployment from the rear of a traveling craft. Zhou et al. showed through OrcaFlex modeling that the sinkage rate was less dependent on the cable buoyancy and ship speed than on the upwelling current of the environmental field.

While drag and buoyancy are well understood topics, the slenderness of the cable is unique and requires specific attention. For the case at hand, the L/D ratio is 2×10^6 for the smallest diameter considered, where L is the cable length. White (1972), which studied the largest L/D ratios in all studies found, stated that his equations for Cd were only validated with experimental work up to $L/D = 5 \times 10^5$. Until the field studies can be used to verify the exact drag coefficient, ESDU 80025 drag coefficients will be used in this study. Cd_T is assumed to be a function of Cd_N and α, given in ESDU 80025 as:

$$Cd_T = kCd_N (\csc^2 \alpha)\alpha \frac{\pi}{180}\left(2 - \alpha \frac{\pi}{180}\right) \quad (6)$$

where k is a coefficient, given as k=0.033 for long, smooth circular cylinders.

3. Parametric Analysis of Two-Section Towed Cable

3.1 Objectives

The experimental model originally proposed would deploy a FOMC (D ≅ 0.0005 m, i.e. 0.5 mm) connected to a drogue chute for tension and a depressor for elevation control (Figure 3). The tow velocity of the ship would vary to alter the drag forces on the cable which ultimately have an effect on the tension, position, deployment depth and attenuation of the signal. The exact dimensions of the fiber were still in development and not yet released; this model provides a parametric analysis for the range of potential values.

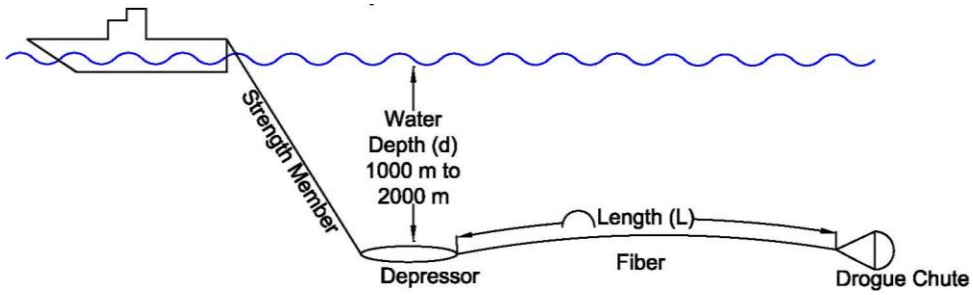

Figure 3. Experiment schematic.

EXWC requested the following objectives be met by this study:

1. Provide a recommended size and weight of the depressor.
2. Provide a recommended size of the drogue chute.
3. Provide a recommended size of the strength member.
4. Derive the tension vs. velocity relationship for the FO cable.
5. Determine the influence of buoyancy on fiber response.
6. Determine the influence of diameter on fiber response.
7. Determine the influence of the water depth.

3.2 Model Setup

The model is idealized by assuming the fiber is attached to a fixed position in the presence of a constant current, V_o, to represent the boat speed. Waves are removed because the cable depth is much deeper the half of the expected wavelength for all cases. Figure 4 shows the model setup. The downdraft end is connected to a neutrally buoyant 3D buoy (three degrees of freedom) to represent the drogue chute. On the updraft end is a depressor suspended from a fixed point by a strength member. The depressor is also modeled as a 3D buoy but negatively buoyant and with drag coefficients representing a sphere. The model environmental depth is set to 4,000 m to not interfere with drag forces.

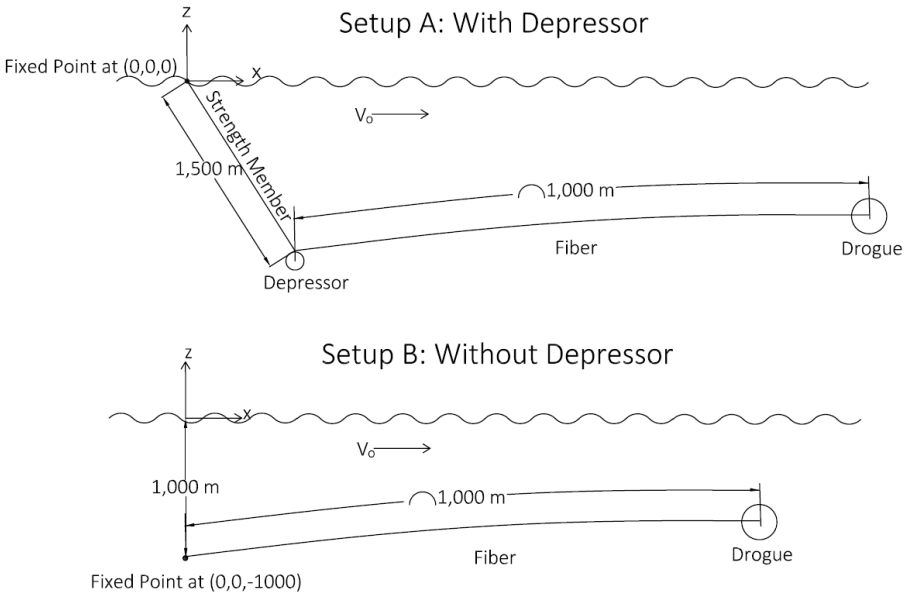

Figure 4. OrcaFlex model setup. Not to scale.

3.2.1 General and Environmental Parameters

Waves were turned off and currents were held constant for this simplistic model. The only dynamic load on the system would be vibration induced vorticities (VIV), but as the cable and

buoy are axisymmetric and traveling in-line with the current, VIV effects were negligible. Therefore, the model was run in steady state only (OrcaFlex calls this a “Statics” run).

General and environmental coefficients were all estimated based on a temperate zone between 500 m and 2500 m and shown in Table 1. Kinematic viscosity, ν, is determined using the SEAWATER toolbox based on Nayar et al. (2016) and Sharqawy et al. (2010). Temperature, T, is assumed constant. The only parameter here that was varied was the current, V_o. The current is vertically uniform as it is representing only the boat speed and the ambient current is assumed to be zero. The base case velocity is 3 m/s. Waves and wind are turned off.

Table 1. General and Environmental Model Parameters.
Range of V_o shown with base case value in parenthesis.

Sea		
ν	1.35E-06	m^2/s
T	10	°C
Re calculation	Nominal	
Sea Density		
ρ	1.034	te/m^3
$\partial\rho/\partial z$	0	
Sea Bed		
h	4000	m
Current		
V_o	0.5 to 5.0 (3.0)	m/s
$\partial V_o/\partial z$	0	

3.2.2 Drag Coefficients

Drag coefficients are derived using the process described in the ESDU 80025 (1986) design guide for flow around a cylinder. Because drag is split between normal and axial components, Cd_N and Cd_T respectively, the cable angle is significant to determine the local Cd. ESDU 80025 provides curve fit equations for drag on inclined cylinders from tangential to axial orientation ($0^o \leq \alpha \leq 90^o$). Figure 5 shows how Cd varies for different angles of inclination. As reference, using flows between 0.5 and 5 m/s and diameters between 0.0005 m and 0.005 m, the range of

Reynolds numbers (V_rD/v) is expected to be between $2x10^2$ and $2x10^4$. The normal drag coefficient is much more sensitive to changes in angle and becomes negligible in axial flow. The cable will be most inclined against flow starting at the depressor and then curve until perpendicular or near perpendicular to flow at the drogue end. The flexible cable will exhibit several different angles along its curvature, but OrcaFlex only allows a single Re vs. Cd_N relationship for each line type and only a single constant value for Cd_T.

As a note of caution when looking up drag coefficients, the Cd_T calculated using ESDU 80025 is based on a drag area of DL while OrcaFlex uses a drag area of πDL for F_T. The Cd_T calculated by ESDU 80025 must therefore be divided by π before using in OrcaFlex. All values used in the paper are based on OrcaFlex's definition of Cd_T for direct input into the model. Care should be taken when comparing Cd values from previous studies that may differ by a factor of π based on how the drag area is defined.

Variations in flow angle along a single line are not possible unless the cable is broken up into discrete sections and each having its own line type assigned with different Re vs. Cd_N curves. This was not attempted but may be examined in future iterations. The Re vs. Cd relationship associated with α=60° is chosen for this project since the steepest angle of attack observed was 65^o in this study. Ideally the cases would be re-run with a new Re vs. Cd_N curve; judging by Figure 5 it may reduce normal drag by as much as 25% in the most extreme cases. But in most cases, including all neutrally buoyant cases, the normal component of velocity is negligible and normal drag is insignificant. The more conservative Cd_N values should have little impact in total tension in near axial flow. A constant value of Cd_T = 0.011 is chosen for the base case using the convergence shown in Figure 5.

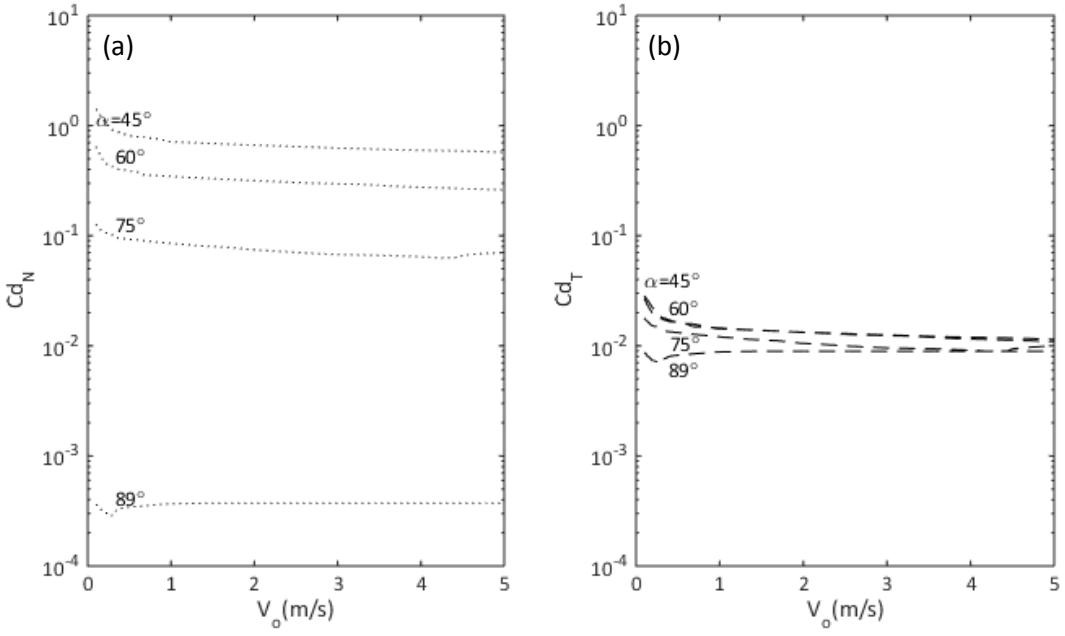

Figure 5. Cd vs. Re for an inclined cable. (a) Cd_N vs. Re. (b) Cd_T vs. Re. D=0.0005 m.

While the fiber is assumed to be smooth glass with surface variations in the range of $\varepsilon=10^{-6}$ m, the small diameter makes the ε/D ratio significant according to ESDU 80025, providing the fiber-optic cable a relative roughness that constricts the turbulent wake reducing friction and shifting the critical Reynolds number, Re_{crit}, to lower values (see Figure 6). Whether this is found to be true or just an artifact of equations derived from larger diameter cables needs to be determined experimentally. In either case, the effects are only significant at speeds less than 2 m/s as shown in Figure 7.

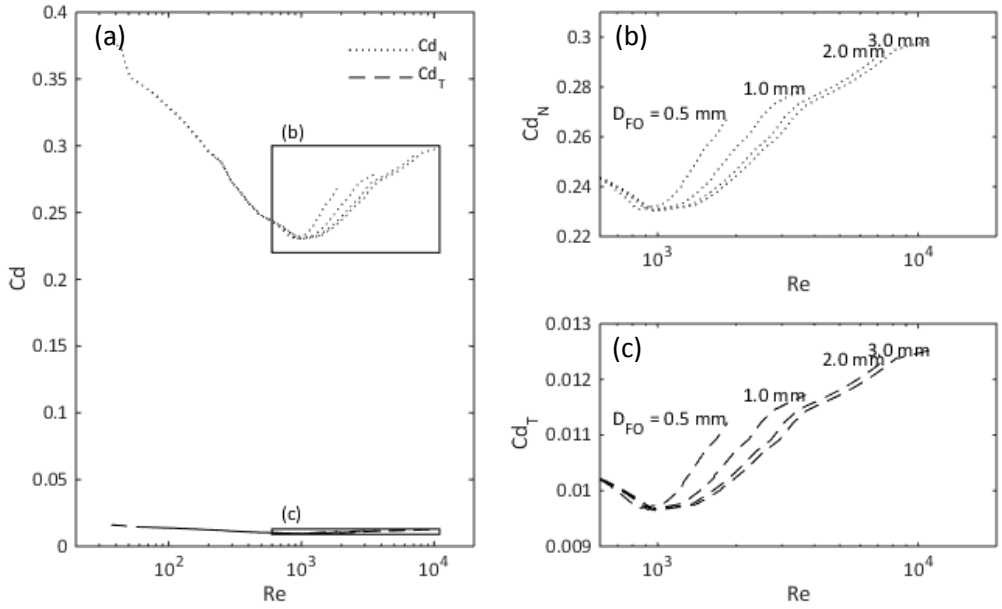

Figure 6. Cd_N and Cd_T vs. Re based on ESDU 80025 for various cable diameters. α=60°.

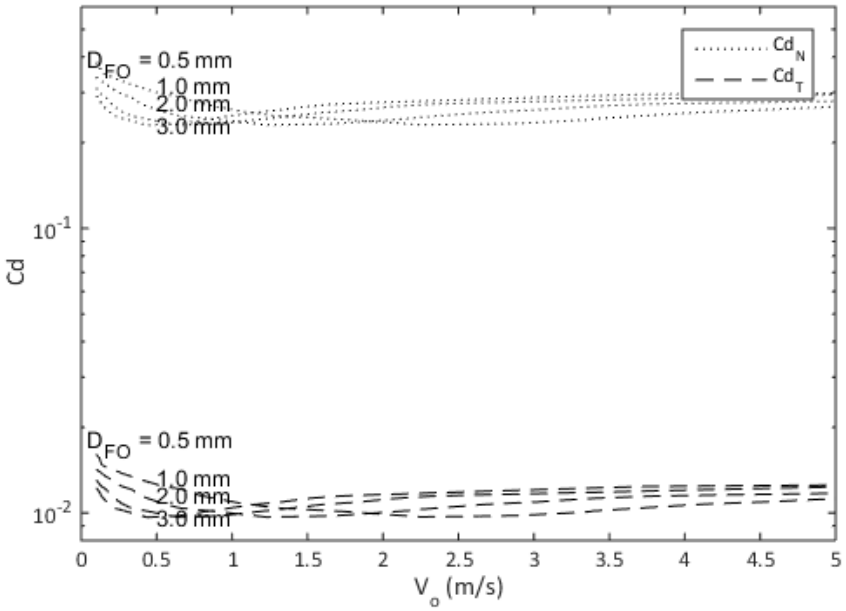

Figure 7. Cd_N and Cd_T vs. V based on ESDU 80025 for various cable diameters. α=60°.

Determining the drag of the drogue is more difficult. Each drogue is unique and manufacturers are reluctant to publish their proprietary drag vs. velocity charts (per phone interview with

Para-Tech Engineering Co., Nov. 16, 2015). Also, the drogue for this experiment that will be used to steady a fiber-optic cable will likely be much smaller than a commercial off the shelf drogue used to arrest a sailing vessel. One drogue drag profile was published for Shewmon truncated cones in a general guide book on drogues (Hinz, 1987) with front opening diameters ranging from 0.61 m (2 ft) to 1.22 m (4ft) and it is reproduced as Figure 8.

Drag on a bluff body is calculated in OrcaFlex by Equation (2) where A is the drogue opening. The Cd values for each point in Figure 8 are calculated using Equation (2) as well as the corresponding Re values. The resulting Re vs. Cd plots for each size drogue are shown in Figure 9. The accuracy, not only of the source but also of the values' applicability to any non-Shewmon drogue is questionable and should be verified with specific data for the drogue used in the experiment. The drogue is modeled as a 3D buoy, only a single Cd is allowed for each cardinal direction. Therefore, the baseline Cd_x in the direction of flow is chosen as 2.0 which is

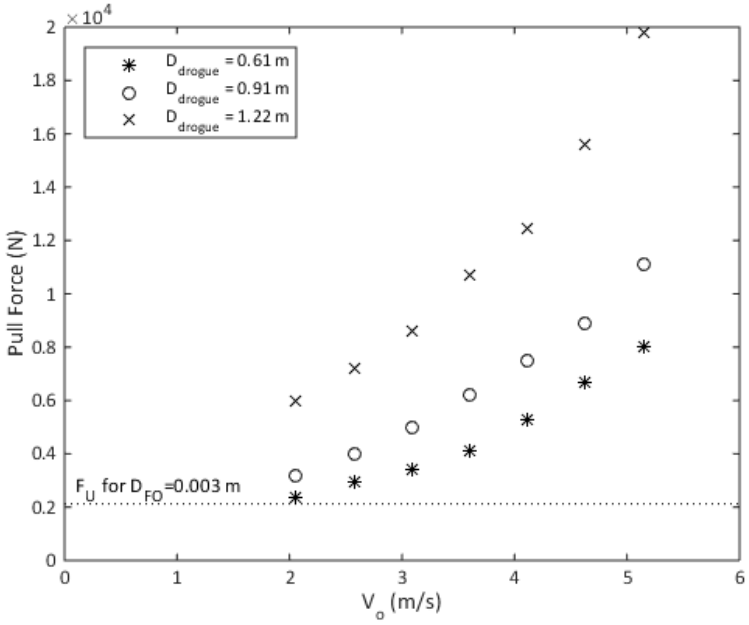

Figure 8. Drag performance of Shewmon truncated-cone drogues (modified from Fig. 27 in Hinz, 1987).

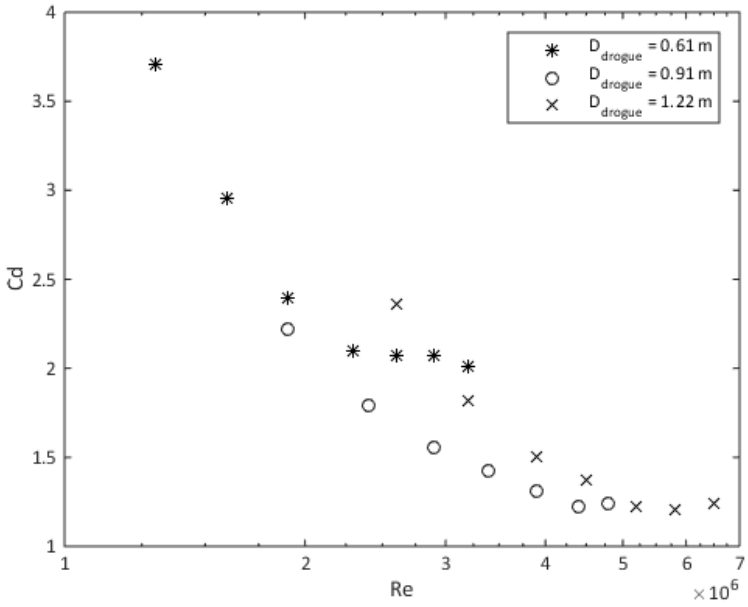

Figure 9. Cd vs. Re for Shewmon truncated-cone drogues.

the asymptote for a 0.61 m drogue and the $Cd_{y,z}$ in the other two directions are arbitrarily chosen to match a subcritical sphere, or 0.4, (Morrison, 2013).

3.2.3 Object Parameters

Table 2 shows the line characteristics. The cable is idealized as an inextensible string and perfectly flexible. Only tensile forces are considered; flexure, shear, and torsion are ignored. Length is held constant while the diameter varies between 0.5 mm and 3 mm, the size of commercially available bare fiber-optic cables. Bare fiber-optic cables produced by Mitsubishi (Mitsubishi Rayon Co., Ltd.) have densities ranging from 774 kg/m^3 to 1,273 kg/m^3. Sea density also varies in nature between 1,023 kg/m^3 and 1,037 kg/m^3 (Kaneko, Takatsuki, Kamiya, & Kawae, 1998). Rather than adjusting both the seawater density and the cable density, the seawater density will be held constant and the cable density will adjust to provide a specific gravity, $\gamma=\rho_{FO}/\rho_W$, between 0.75 and 1.25. The cable is assumed flexible and with negligible

torsional strength over the length. Drag coefficients are prescribed as discussed above. OrcaFlex limits lines to a single value for Cd_T, which is 0.011 for the base case, and a single Re vs. Cd_N curve for normal drag which was calculated using the conservative $\alpha=60^o$. The segment length is the length of the cable elements that are treated as single lump masses. The base case, with all γ_{FO} , was run using a segment lengths of 0.5 m, 5 m, and 50 m and there was zero difference in tensions or end locations out to six significant digits. A segment length of 5 m was chosen for all cases.

The parameters of the strength member line are found using OrcaFlex's line wizard based on a stock 1/2", 6x19 Wire Rope. A 1/2" nominal diameter 6x19 IPSWSC or IWRC wire rope has a nominal strength of 23,000 lbs (Commander, Naval Sea Systems Command, 2000) which equates to a safe working limit (SWL) of:

$$\text{SWL} = \frac{23{,}000 \text{ lbs}}{(\text{S.F.} = 5)} * \frac{1}{2} \text{ (for dynamic loads)} = 2{,}300 \text{ lbs or } 10.2 \text{ kN}$$

This provides sufficient strength to support a 5 kN (0.5 te) depressor and the approximately 1 kN tension from the fiber-optic cable and drogue. Remaining parameters are unchanged from the OrcaFlex template. The strength member was not a focus of study since the depressor elevation can be directly controlled by the winch operator by reeling in or paying out additional line.

The small size of the cable makes selecting a proper drogue difficult. Assuming the ultimate stress of the to-be-designed FOMCs matches the average ultimate stress of Linden Photonics, Inc.'s existing STOFCs, the ultimate stress will be only 0.3 GPa (Linden Photonics, Inc., 2014). For the range of diameters used in this study, and the corresponding ultimate strength ratings, F_u, are provided in Table 3.

Table 2. Line Properties
Range of D_{FO}, γ_{FO}, and Cd_T shown with base case values in parentheses.

Fiber Optic Cable	Geometry and Physical Characteristics		
		L	1000 m
		D	0.0005 to 0.003 (0.001) m
		γ	0.75 to 1.25 (1.00)
		Segment length	5 m
		Torsion	Excluded
	Drag & Wake		
		Drag Formulation	Standard
		Reacts to Wake	Yes
		Cd_N	varies w/ Re
		Cd_T	0.006 to 0.016 (0.011)
		Ca_N	1
		Lift	Excluded
Strength Member	Geometry and Physical Characteristics		
		L	1500 m
		D	0.01 m
		ρ	0.00058 te/m
		dL	10 m
		Torsion	Excluded
	Drag & Wake		
		Drag Formulation	Standard
		Reacts to Wake	Yes
		Cd_N	1.2
		Cd_T	0.008
		Ca_N	1
		Lift	Excluded

Table 3. Ultimate Strength of Cables

D_{FO} (m)	F_U (N)
0.0005	59
0.001	236
0.002	942
0.003	2121

The base case 1 mm cable will snap at 236 N which will easily be snapped by the smallest Shewmon truncated drogue. Hypothetical drogue sizes of 0.15 m, 0.23, and 0.305 m (6 in., 9 in., and 1 ft, respectively) are used to provide a reduced force, but further research is needed to verify if drogues of this size still function as intended.

Table 4 provides the input parameters for the two buoys, the drogue and depressor. Drag coefficients are set at 2.0 as described earlier. The added mass coefficients Ca from the Morison Equation (Morison, O'brien, Johnson, & Schaaf, 1950) can be ignored because the model is run as a steady state, but for completeness, the coefficient is set to 0.5 similar to a sphere.

The depressor is modeled as a spherical lump mass with a 0.305 m (1 ft) diameter. Drag is set to 0.4 to correspond with a sphere in subcritical flow (Morrison, 2013) and Ca is the same as for the drogue.

Table 4. Buoy Properties
Range of D_{drogue} and $M_{depressor}$ shown with base case values in parenthesis.

Drogue	Geometry and Physical Characteristics			
		D	0.15 to 0.31 (0.23)	m
		γ	1	
	Drag			
		Cd_x	2	
		$Cd_{y,z}$	0.4	
		$Ca_{x,y,z}$	0.5	
Depressor	Geometry and Physical Characteristics			
		D	0.305	m
		Volume	0.0148	m^3
		M	0.05 to 0.25 (0.2)	te
	Drag			
		$A_{x,y,z}$	0.073	
		$Cd_{x,y,z}$	0.4	
		$Ca_{x,y,z}$	0.5	

3.3 Test Matrix

A parametric analysis was performed to analyze the effect different variables had on the resulting forces and elevation of the fiber-optic micro cable. The ranges and variables tested are shown in Tables 1 to 3. Velocity and specific gravity were judged to have the greatest impact and were varied with all other variables. Velocity ranged in 10, 0.5 m/s increments. Specific gravity was tested at 0.75, 0.90, 1.00, 1.10, and 1.25. In all, there were 50 tests performed each time one of the other four variables (FO cable Cd_T, FO cable diameter, drogue diameter, depressor mass) varied. A total of 750 cases were run in statics mode to find the equilibrium position in a constant flow field.

Results analyzed from each case include the:

1. Tension in the end of each line.
2. Maximum tension in each line.
3. Depth and position of the depressor.
4. Depth of position of the drogue chute.
5. Highest and lowest point of the fiber-optic cable.
6. Force on the drogue.

3.4 Results and Discussion

3.4.1 Qualitative Observations

In Setup A, with the FOMC attached to a depressor, the depressor rose in elevation with velocity along an arc-shaped trajectory whose radius roughly corresponded to the length of the strength member. Figure 10 shows all the positions of the base case. The strength member was not taught, but concave down. The FOMC was horizontal when neutrally buoyant, concave down when positively buoyant, and concave up when negatively buoyant. The highest angle of attack occurred at the depressor and then every case reached horizontal at the drogue end. At low speeds when tensions where lowest, the drogue end traveled furthest from horizontal. At speeds greater than 3 m/s, the FOMC appeared horizontal for all cable densities. When run as Setup B, results were the same except the left most point remained fixed at the origin as designed making results easier to analyze.

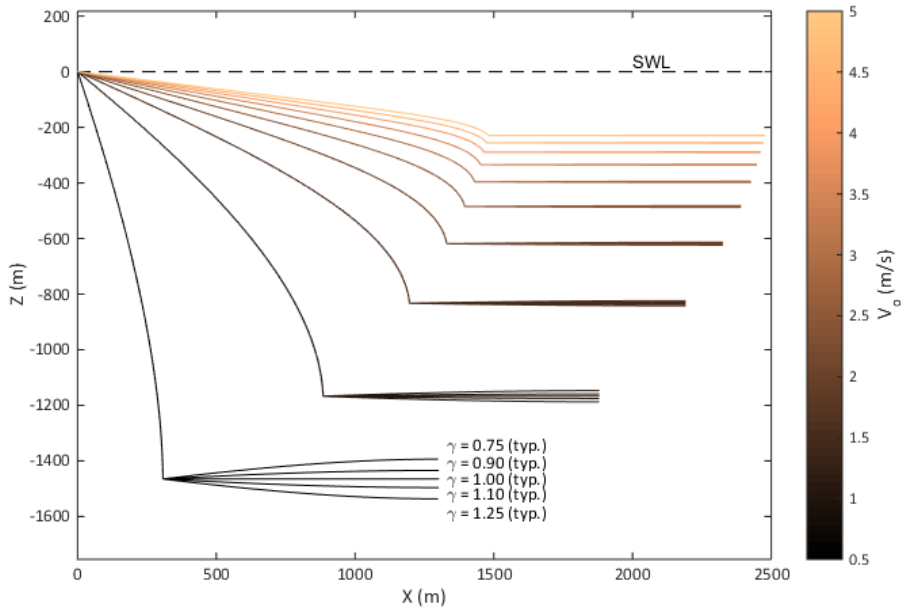

Figure 10. Steady-state equilibrium of strength member and FOMC for base case parameters, Variations in FOMC density and ship speed.

3.4.2 Velocity and Cable Density

Velocity and cable density were varied for each case in the study. The 50 combinations of five densities and ten velocities for the base case provided a baseline for the study that was then altered one at a time for each additional permutation. As discussed above, drag is proportional to velocity squared. Figure 11 shows the tension in the FOMC at the depressor end at different velocities. The total tension in the cable is not affected by the specific gravity. As the local inclination of the curved cable changes, there is a transition from normal to tangential forces which are not equivalent. However the small difference is insufficient to make any discernable difference in the total tension of the cable.

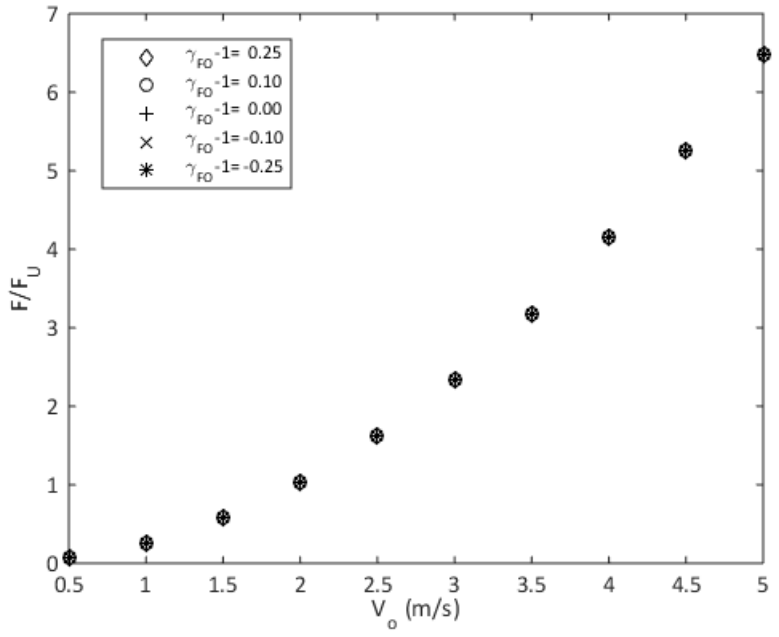

Figure 11. Cable tension at the depressor end for varying velocities and specific gravities.

When this analysis was conducted, EXWC was still in the planning process with regards to whether the FOMC would be dragged from a depressor or deployed behind an ROV. If an ROV were to be used, in order to stay "on station" at a prescribed depth the upward or downward force caused by a positively or negatively buoyant towed FOMC would have to be overcome by the ROV's ballast, thrusters or wings. Table 5 provides the wet weight, or net buoyant force of the 1,000 m FOMC for various diameters and specific gravities. It is expected that these forces will be altered by the velocity and tension in the cable.

Table 5. Wet Weight (N) of the 1000 m FOMC (positive upwards)

γ	D_{FO} (m)			
	0.0005	0.001	0.002	0.003
0.75	0.50	1.99	7.97	17.93
0.90	0.20	0.80	3.19	7.17
1.00	0.00	0.00	0.00	0.00
1.10	-0.20	-0.80	-3.19	-7.17
1.25	-0.50	-1.99	-7.97	-17.93

For the base case, Figure 12 shows vertical force at the depressor end, F_Z, versus the drag velocity for each specific gravity. F_Z is normalized by the new buoyant force. By definition, the larger magnitude specific gravities have greater buoyant force. The velocity assists in creating drag in the direction of the cable, which is inclined to start with, providing an increasing force component in the vertical. After reaching near axial flow at about 2.5 m/s, however, increases in velocity and drag only pull horizontally and not vertically.

At the other end of the FOMC is the depressor. In every case, the depressor was assumed neutrally buoyant and therefore was the highest or lowest point of the FOMC. The vertical distance of the drogue from a pure axial flow position is denoted as ΔZ (see the inset in Figure 13). Figure 13 shows the steady state position of the drogue, normalized by the length of the cable, for different velocities and cable densities. ΔZ is shown to be linearly proportionate to γ-1 while being inversely proportionate to V_o^2. The drag force on the cable, whether applied at the end through a drogue or along the cable as tangential and normal drag, is the only force on the cable that will reduce the ΔZ excursion.

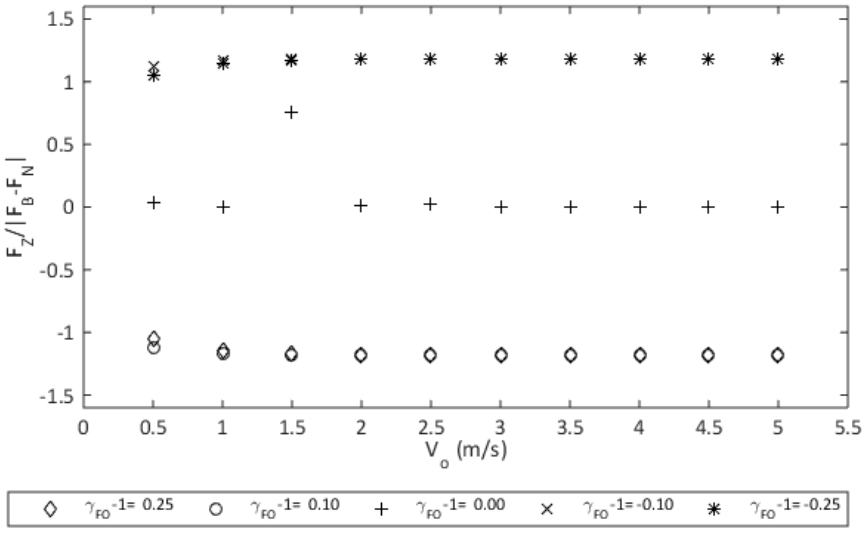

Figure 12. Vertical force on the FOMC at the depressor end for varying velocities and cable densities.

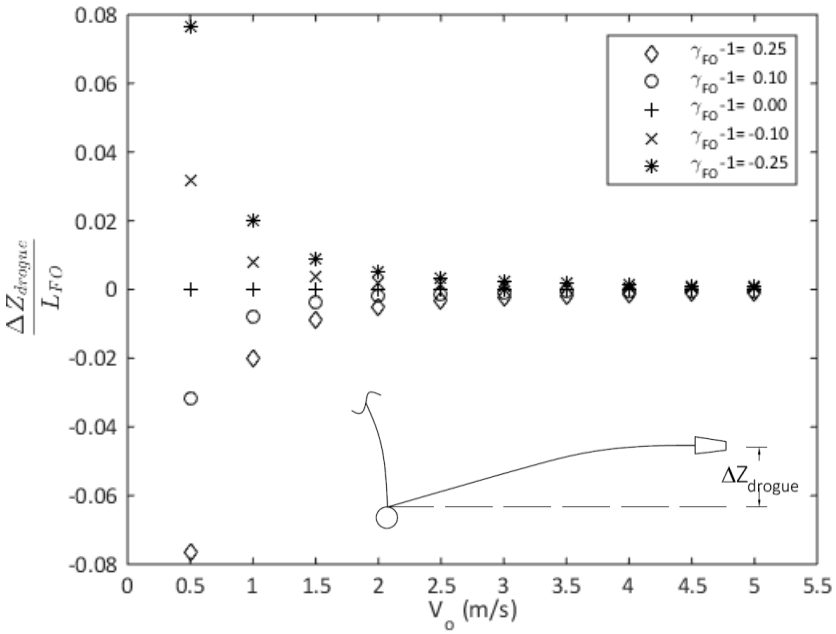

Figure 13. Drogue elevation for varying velocities and cable specific gravities.

When run in the setup with a depressor present, the depressor experienced minor effects from the change in buoyancy. Figure *14* shows on the left side the absolute depth at each velocity. The variable $\Delta Z^*_{depressor}$ is defined as the difference in the resulting depressor elevation from the depressor elevation in the base case (i.e., γ_{FO}= 1, D_{FO}= 1 mm, D_{drogue}= 0.23 m). The origin of $\Delta Z^*_{depressor}$ therefore changes with each velocity. As expected, the changes in cable buoyancy cause a direct rise of the depressor, but the rise is only a fraction of a meter over the ~250 m to 1500 m depth. As the velocity increases, this vertical change decreases substantially with increased tension in the FOMC.

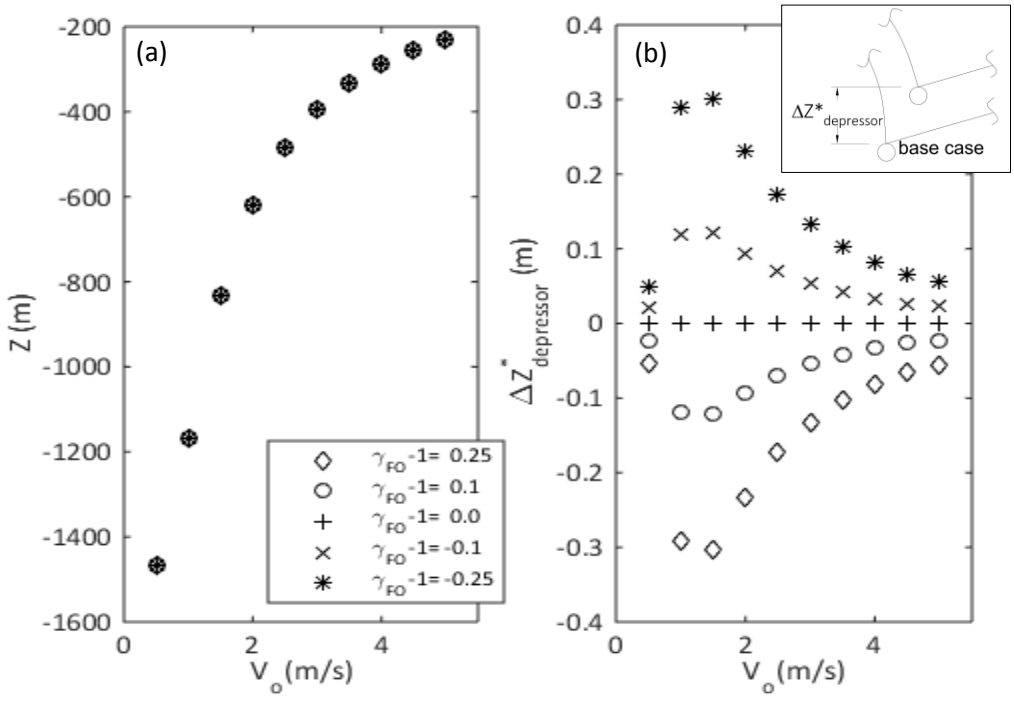

Figure 14. Depressor elevation for varying cable densities. ΔZ^*drogue represents the change from the base case (γ_{FO}-1= 0). (a) Absolute elevation; (b) Elevation in relation to the base case.

3.4.3 Drogue Diameter

For the parametric study, the first parameter analyzed was the drogue diameter. Although it was not a focus to completely model all aspects of the drogue, EXWC asked for a recommended drogue size for the physical experiment. Figure 15 shows that tensions increased not only with V_o^2, but also with D_{drogue}^2. In order to keep the FOMC tension below F/F_U=1.0, EXWC should use a 0.23 m (9" drogue) traveling at less than 2.0 m/s. To reach the stability criteria of $\rho\pi D_{FO}^2 V_o^2/4$, a 1 mm cable traveling at the extreme 5 m/s would require only 0.02 N of tension on the free end (or about 0.005 lbs.).

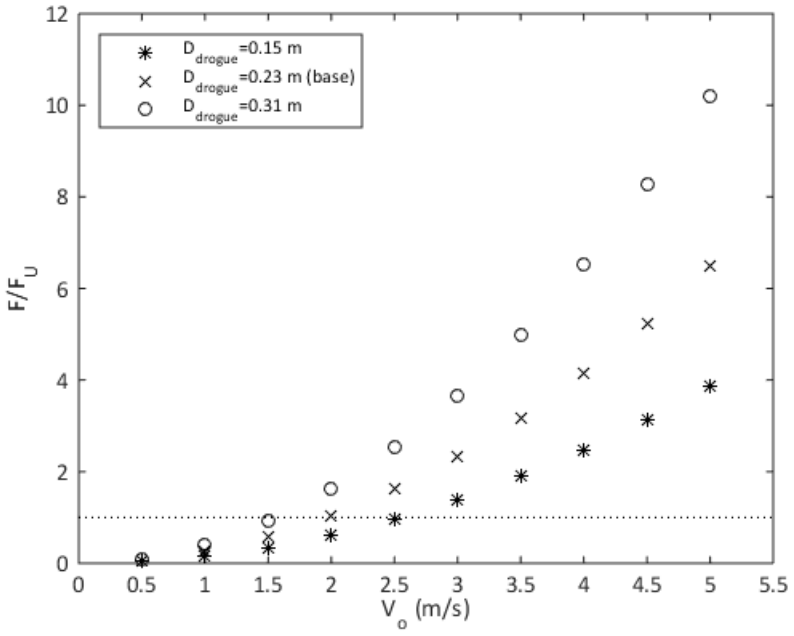

Figure 15. Max tension in FO cable for varying drogue diameters.

Figure 16 shows the inverse relationship of the drogue diameter and the elevation change of the drogue end. The drogue elevation is again inversely proportionate to the drag, which

increases by a factor of D_{drogue}^2. The reduction in tension at the drogue end appears to have limited impact on the elevation change.

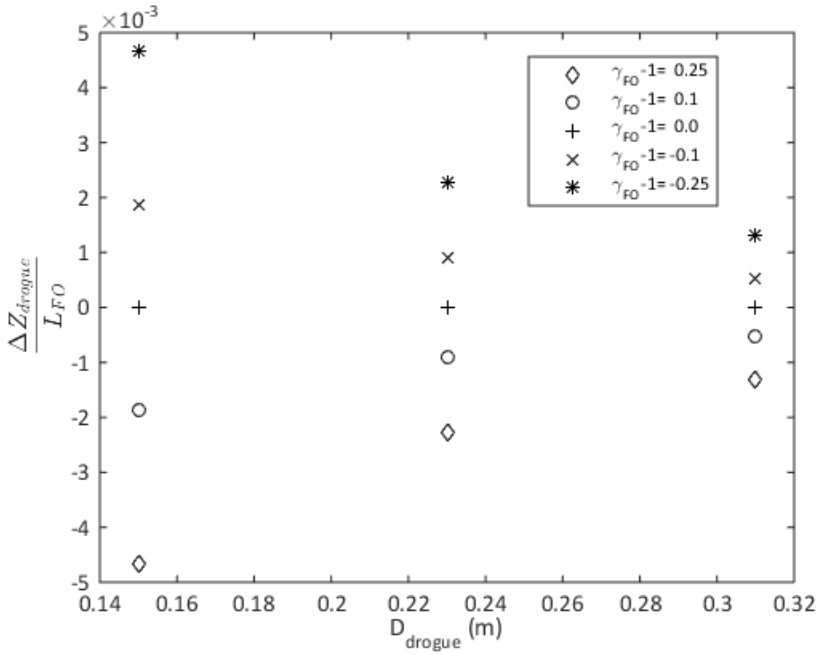

Figure 16. Elevation change between depressor and drogue end of FOMC for various drogue sizes and FOMC densities. V_o = 3 m/s.

The depressor reacted to this increased tension by the drogue by raising in the water column for larger drogues as shown in Figure 17. Up to about 1.5 m/s, the increased tension caused by the drogue causes the depressor to rise higher than the base case. Then from 1.5 m/s and faster, the $\Delta Z^*_{depressor}$ drops and approaches the same elevation as the base drogue size. It was expected that the system would then converge around $\Delta Z^*_{depressor}$ = 0 m, but instead the depressor drops below the base case.

The drop in elevation is caused by reduced curvature in the strength member as shown in Figure 18. When the horizontal force of the FOMC is increased, such as by using a larger drogue, while the vertical force of the depressor stays constant, to reach a new equilibrium the tension in the strength member must pull at the node at a lower angle. A lower angle is

achieved by either rotating the strength member around the origin, causing the depressor to rise, or by elongating the chord length and reducing the curvature in the strength member causing the depressor to fall. Curvature in the strength member is increased by normal drag and decreased by its weight and tension. When the strength member is more axial, there is a decrease in normal force, allowing curvature to reduce sufficiently that rotation is not needed to reach a new equilibrium. This decrease in normal force is what appears to be happening at around 4 m/s.

This shows that beyond some critical velocity, the added tension in the FOMC stretches the depressor strength member into a deeper depth. Evaluating further to do a parametric analysis for determining this critical velocity is beyond the scope of this project. Similarly, since this study does not focus on a full evaluation of the strength member and depressor, the critical velocity shown in Figure 17 at 4 m/s cannot be assumed to be accurate. What this does show is that there is a critical velocity when further increases in tension in the FOMC can slightly increase depth rather than reduce it.

Since the cable has zero flexure and can only provide a force in the direction of the local angle of attack, a highly tensioned cable acting in pure axial direction will have little to no vertical lift force on the depressor. Figure 19 shows how F_Z compares to the drogue diameter for different specific gravities. Similar to before, the increased drag is inversely proportionate to F_Z. When F_Z is normalized with the net buoyant force from Table 5, the different densities collapse on one another. Other than altering the net buoyant force, the vertical force is not proportionate to the density. Since buoyancy and weight are constant for all speeds, Figure 19 shows us that the vertical component of the drag force is about 37% of the net buoyant force for the smallest drogues, but this reduces to just 11% when the drogue size is increased to 0.31 m.

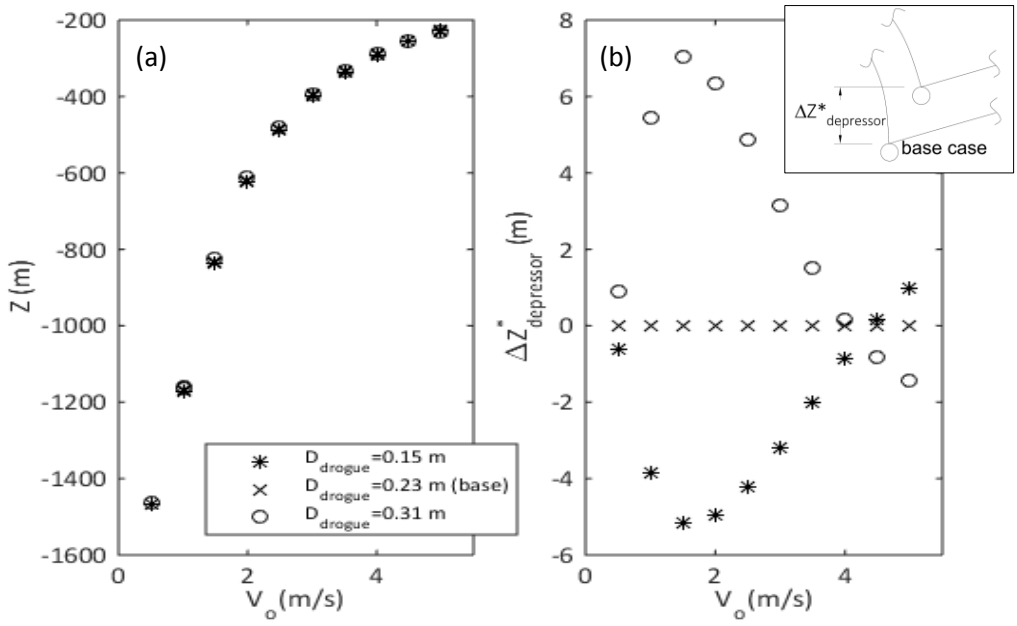

Figure 17. Depressor elevation for varying drogue diameters. ΔZ^*_{drogue} represents the change from the base case (D_{drogue}=0.23 m). (a) Absolute elevation; (b) Elevation in relation to the base case.

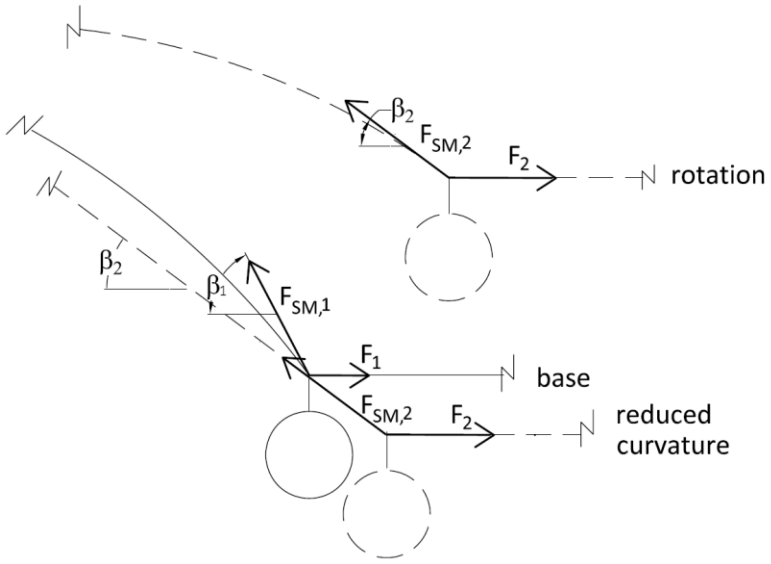

Figure 18. The angle of the strength member tension, β_1, must decrease to β_2 when the tension in the FOMC, F_1, increases to F_2. This is done by either the strength member rotating counter-clockwise causing the depressor to rise, or by reducing curvature in the strength member causing the depressor to sink.

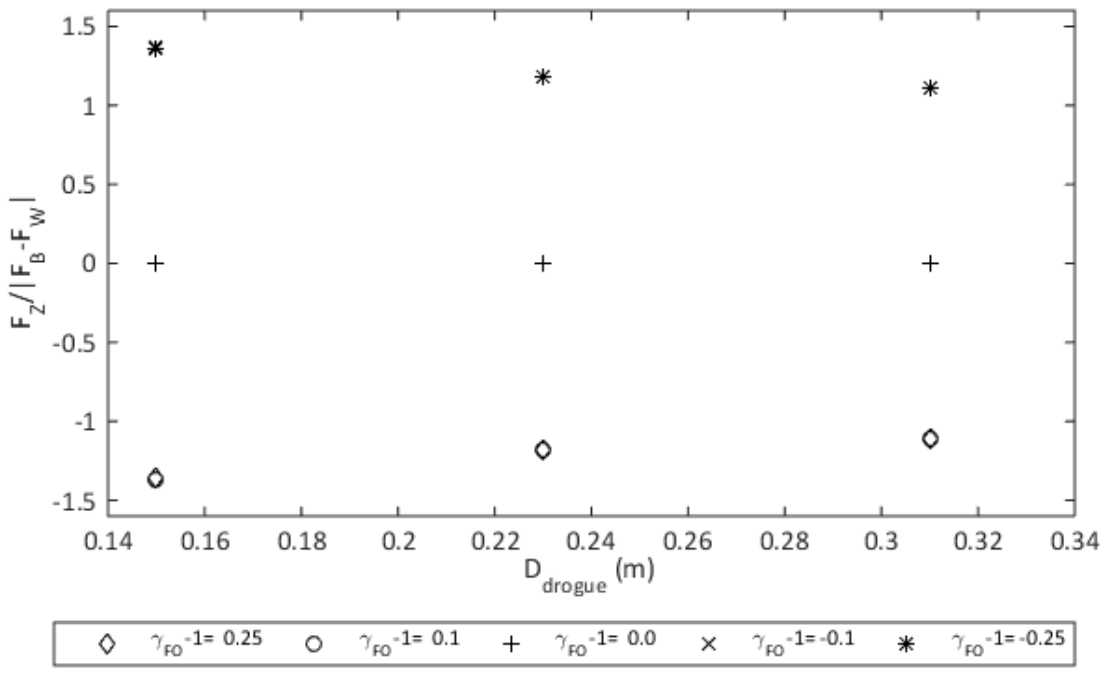

Figure 19. Vertical lift force on the depressor end of the FOMC for various drogue sizes.

3.4.4 Tangential Drag Coefficient

Variations in Cd_T resulted in similar changes produced by D_{drogue} with a few exceptions. The max tension in the cable (Figure 20) has a linear relation with Cd_T rather than quadratic which is representative of Equation (2). If the FOMC is assumed to be axial, the ratio of tangential drag, F_T, to the pull force of the drogue, F_{drogue}, is equal to $4Cd_TD_{FO}L/(Cd_{drogue}D_{drogue}^2)$. For the base case, F_T is 41% of the drogue pull force. Because the tension is dominated by the drogue, small changes in the skin drag along the length of the cable result in only minor changes in overall tension. Further fine tuning and experimentation of Cd_T is likely unnecessary if deployment includes a mechanism for providing tension at the free end, such as with a drogue or by attaching the FOMC to some other external device.

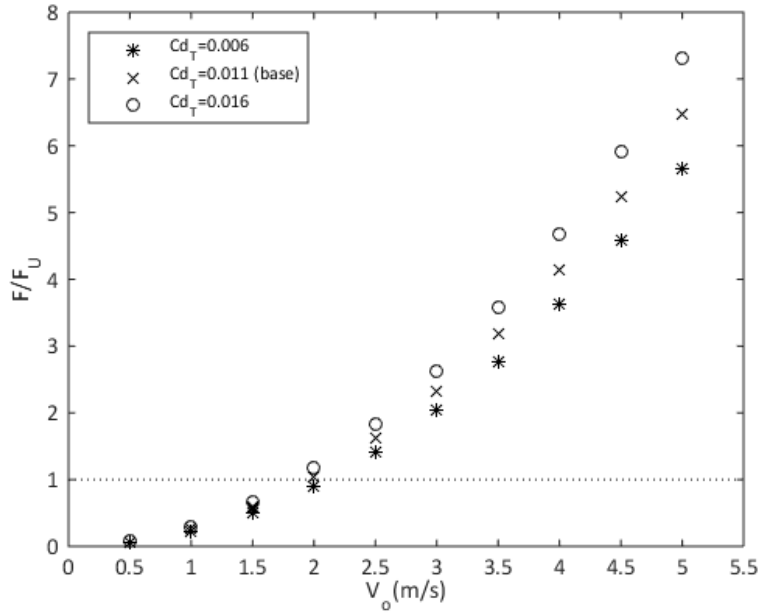

Figure 20. Max tension in FOMC for varying tangential drag coefficients.

Figure 21 shows the change in elevation between the depressor and drogue for varying Cd_T. It demonstrates, as did Figure 16, that increases in tension in the FOMC straighten out the cable. The smaller changes in tension caused by Cd_T have a smaller effect on ΔZ_{drogue} than D_{drogue}.

Figure 22 shows that Cd_T has a positive relationship with $|F_Z|$; this is opposite the effect of drag forces placed on the end of the cable. Because the skin drag acts parallel to the cable and along the entire length, and not only in the direction of flow like the drogue, increases in Cd_T will linearly increase $|F_Z|$.

When run in Setup A, the depressor changes elevation with nearly exactly the same local maxima, minima, and zero-crossing velocities as were exhibited by changes in drogue size. This confirms the previously stated idea that the critical velocities are set by the strength member and depressor rather than the tension in the FOMC. As shown before, the system continues to be less sensitive to Cd_T than other parameters.

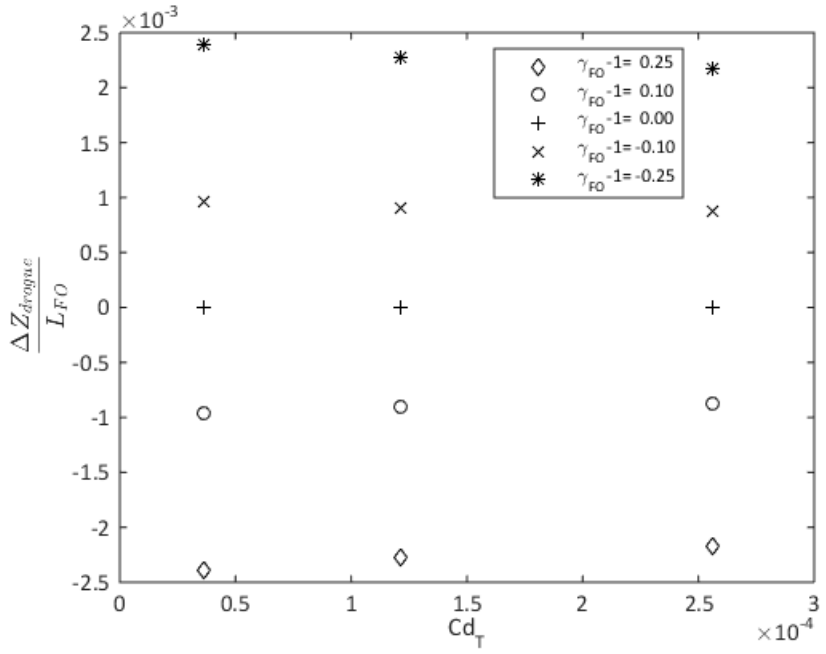

Figure 21. Elevation change between depressor and drogue end of FOMC for various tangential drag coefficients and densities.

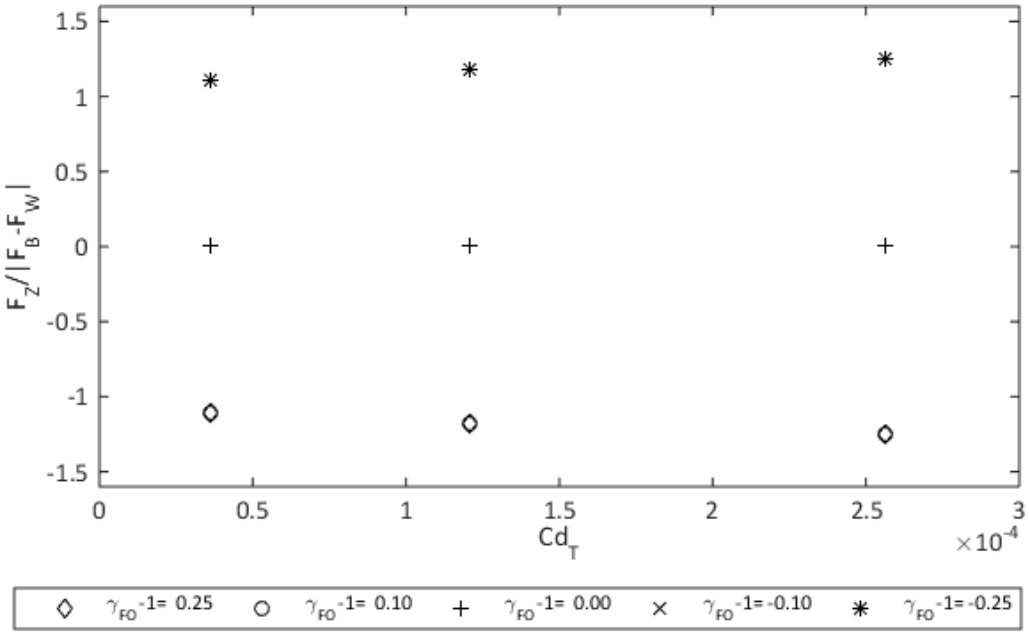

Figure 22. Vertical lift force on the depressor end of the FOMC for various tangential drag coefficients.

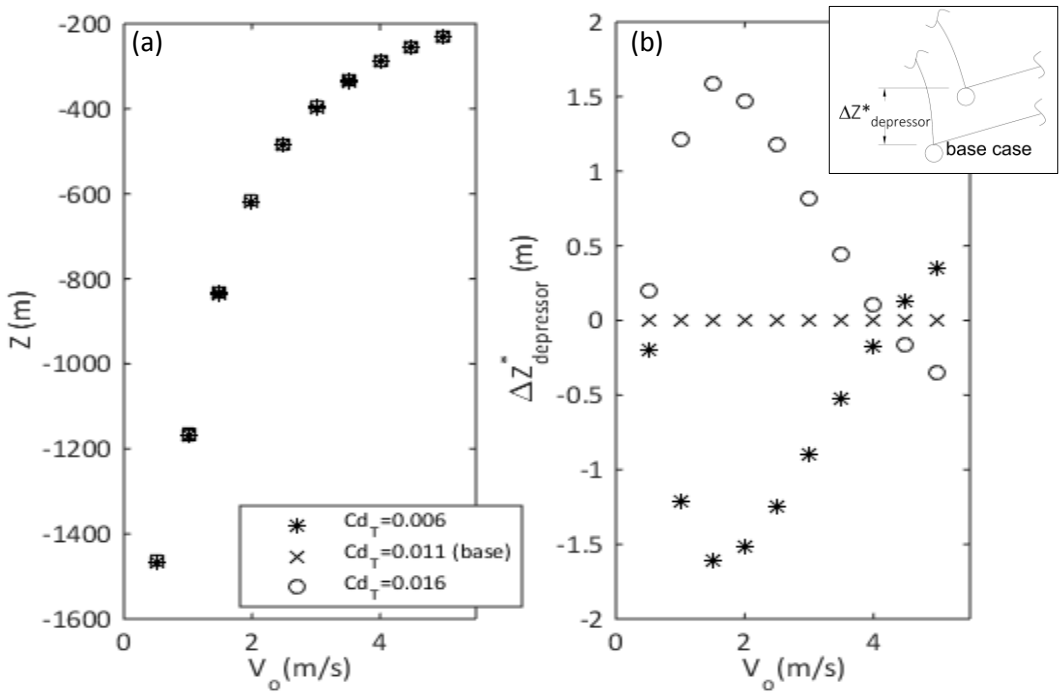

Figure 23. Depressor elevation for varying tangential drag coefficients. (a) Absolute elevation; (b) Elevation in relation to the base case.

Even for a system in pure or near pure axial drag, the system is insensitive to the tangential drag coefficient due to the overpowering drag at the end. If the free end tension is reduced by using a very small drogue, it is likely that the skin drag will become more important. But in the present experimental setup, a Cd_T=0.011 appears to be adequate to provide reasonable results.

3.4.5 Cable Diameter

Cable diameter effects the system in a few ways. First, the increased projected area and surface area increase the normal and tangential drag forces linearly, as shown by Equations (3) and (4). Second, the increased diameter increases volume which in turn increases buoyancy. Total drag is only increased linearly with diameter, as seen in Figure 24.

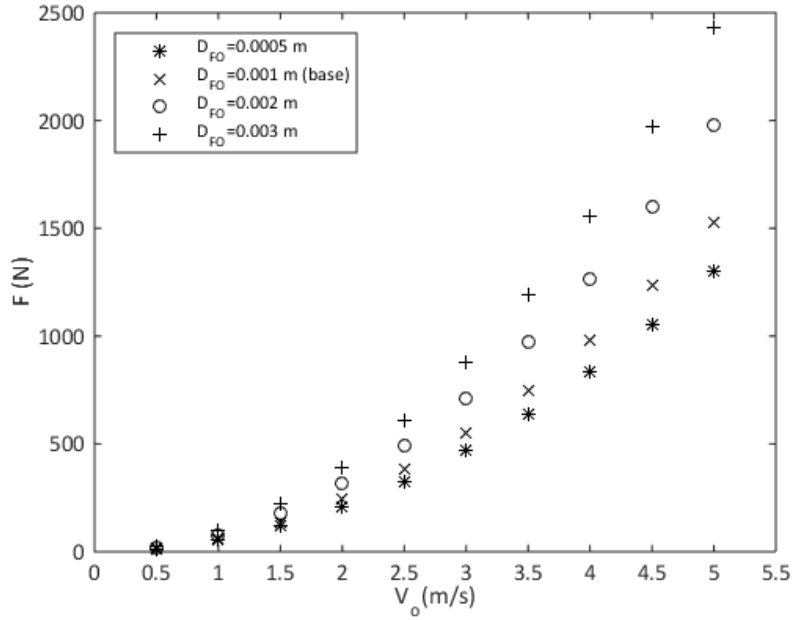

Figure 24. Max tension in FOMC for varying velocities and cable diameters.

When the cable tension is normalized with ultimate strength of the cable in Figure 25, the larger cable is able to withstand an exponentially greater tension. The ultimate strength of the cable increases by D_{FO}^2 which overcomes the linearly increasing tangential drag. Breaking force is not reached until velocities higher than 3.5 m/s for D_{FO}>= 0.002 m.

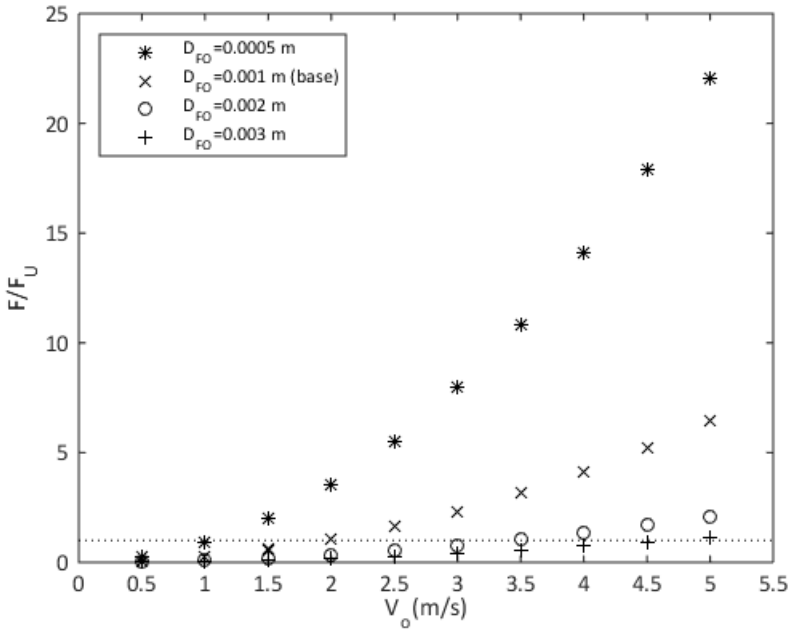

Figure 25. Normalized max tension in FOMC for varying velocities and cable diameters.

Figure 26 demonstrates the large divergence in drogue elevation for various cable diameters. Because volume increases exponentially by a power of three, the linearly increasing drag is insufficient to control the dominating force of buoyancy, and the drogue rapidly rises. This again has no affect if the FOMC is neutrally buoyant, but any variation from neutral buoyancy is compounded by changes in cable diameter.

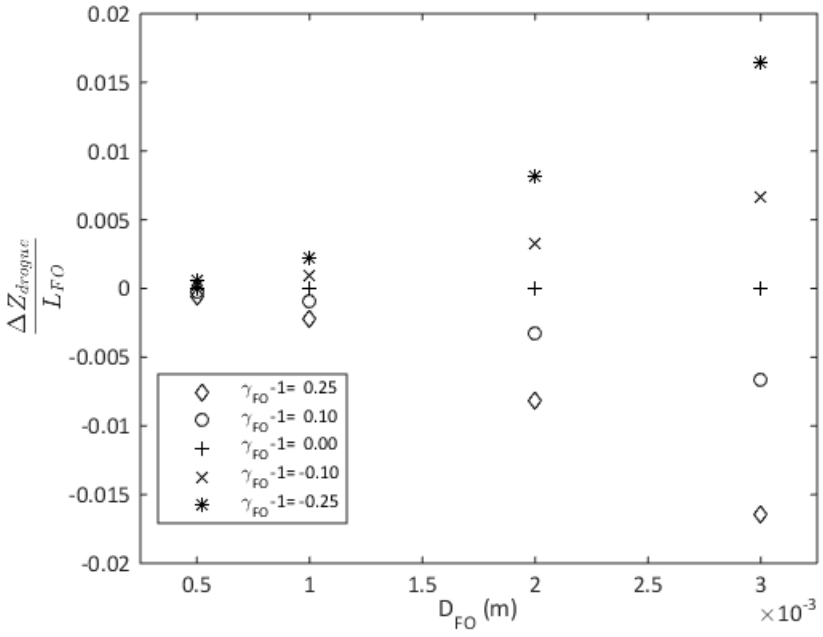

Figure 26. Elevation change between depressor and drogue end of FOMC for varying cable diameters and densities.

Figure 27 shows that the vertical force on the depressor end increases exponentially with FOMC diameter for semi-buoyant cables. The increases in ΔZ inclines the FOMC so that the tension in the cable acts in a more vertical direction on the depressor. The buoyancy forces upward and the drag forces tangential to the FOMC are also increased as discussed, combining for an exponentially increased upward force on the depressor. A neutrally buoyant cable provides no upward force regardless of the size because it remains horizontal to flow.

Figure 28 shows the effects of diameter and density on the elevation of the depressor when dragged at different speeds. The increases in F_z for larger diameter cables were extremely small; a 3 mm cable traveling at 3 m/s, the Fz was only 0.025 N (i.e. 0.005 lbs). But these small changes in upward force amounted to as much as 10 m in elevation change. The combined

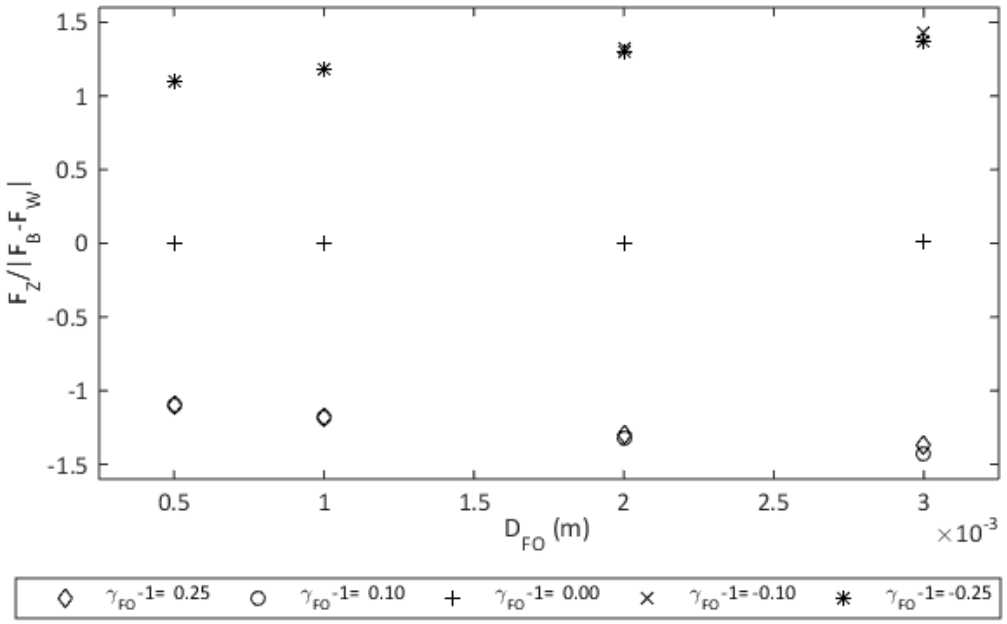

Figure 27. Vertical lift force on the depressor end of the FOMC for varying cable diameters and densities.

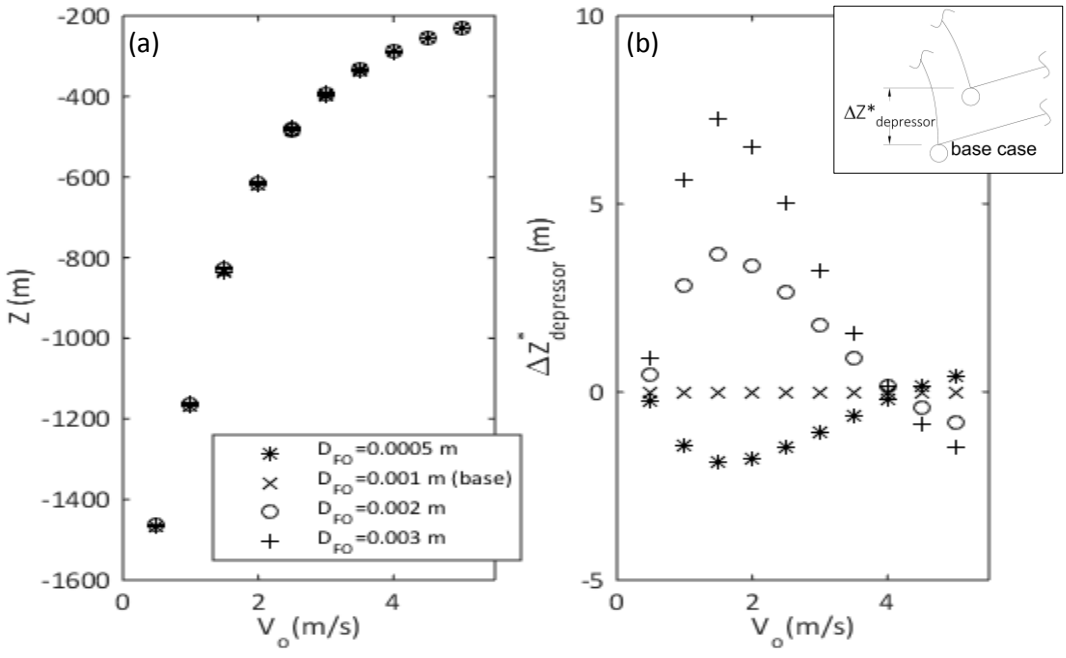

Figure 28. Depressor elevation for varying cable diameters and densities. (a) Absolute elevation; (b) Elevation in relation to the base case.

effect of buoyancy and diameter had its greatest effect at lower speeds until the drag force pulled the cable into a horizontal profile as seen before.

3.4.6 Depressor Mass

The effect of different depressor masses was evaluated upon request from EXWC. The depth does not change the FOMC response since the range of depths that may be experienced in the physical trial are assumed to have constant temperature, viscosity, and density, making depth changes have no effect on the shape and tension of the FOMC. The depressor was evaluated in this study only to recommend a depressor mass size to use in the physical experiment.

Figure 29 shows the various depths of depressors with different masses being pulled at the indicated speeds. The depths vary as much as 321 m but this depth is recovered by a change in velocity of only 0.5 m/s. At higher velocities of the test, even the largest depressors are unable to maintain the specified depth of 1,000 m. To get the specified depth of 1,000 m without having to pay out even more of the strength member, a more streamlined strength member cable or depressor is needed. This was not further tested after the plans for the physical experiment changed to do away with a depressor all together. Based on the load capacity of the barge or boat, the largest depressor that can be safely handled is recommended.

As a note, the depressor buoy was modeled as a 0.15 m (0.5 ft) diameter sphere. In this study, the 0.25 te depressor provided 235 kg (518 lbs) of negative buoyancy.

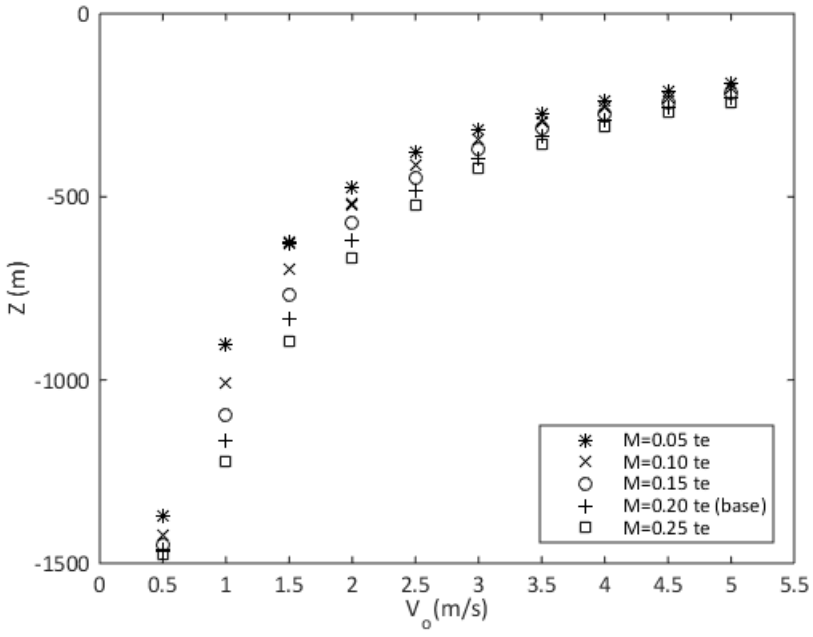

Figure 29. Depressor elevation for varying depressor masses.

3.4.7 Equation for Drogue Elevation

By considering drogue elevation, ΔZ, to be a function of cable length, L_{FO}, cable diameter, D_{FO}, tangential drag, Cd_T, ship speed, V_o, and the diameter of the drogue, D_{drogue}, a non-dimensional equation can be derived. Based on the previous discussion, ΔZ is proportional to (γ-1), D_{FO}^2, $1/Cd_T$, V_o^2, and $1/D_{drogue}$. This can be non-dimensionalized by dividing ΔZ by L_{FO} and using the constant of gravity, g. This gives an equation with the form:

$$\frac{\widehat{\Delta Z}}{L_{FO}} = -A\, g\, \frac{(\gamma_{FO} - 1)\,(D_{FO})^2}{Cd_T\,(V_o)^2\,D_{drogue}} \qquad (6)$$

where A is a constant. Using linear regression, A=12 provides a good fit as shown in Figure 30. The solid line shows a one-to-one slope. The R^2 value is 0.9132. This equation was not tested for different cable lengths, but for the system in question it should provide reasonable predictions of the drogue's excursion from the horizontal plane. Equation (6) starts to over

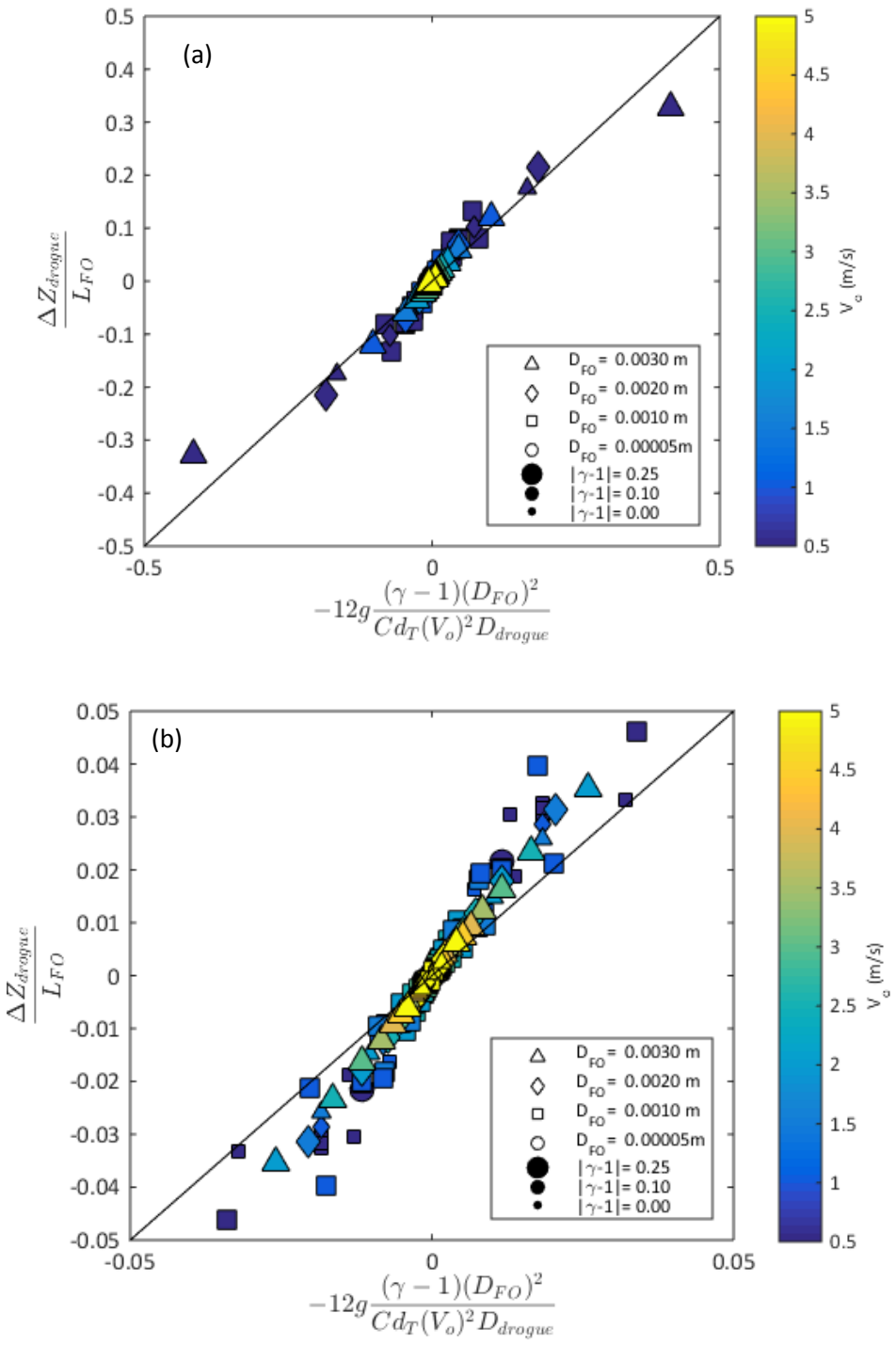

Figure 30. Non-dimensional relationship for ΔZ. Subplot (a) All cases; (b) Zoomed into the -0.05 to 0.05 range.

predict the excursion for large, buoyant cables traveling at low speeds. One possible explanation for this is the curvature of the cable increases allowing the FOMC to stray further from being a taught, straight line.

3.4.8 Equation for Maximum Tension on the Cable

Tension in the cable increased from the drogue to the depressor as each additional downstream length of cable added drag. The forces on each section can be estimated to be the sum of tangential drag force, normal drag force, buoyancy, F_B, weight, F_W, and the drag force of the drogue, F_{drogue}. Buoyancy and weight only act in the z-direction and the drogue only acts in the x-direction. Drag forces have components in both the x and z directions when the cable is inclined. If the cable is assumed to have a constant slope, $\hat{\alpha}$, from the depressor to the drogue, the forces on the depressor end of the cable can be estimated as:

$$\widehat{F_X} = F_N \cos(\hat{\alpha}) + F_T \sin(\hat{\alpha}) + F_{drogue} \tag{7a}$$

$$= \frac{1}{2} \rho Cd_N (D_{FO} L_{FO}) |V_o| V_o \cos^3(\hat{\alpha}) + \frac{1}{2} \rho Cd_T (\pi D_{FO} L_{FO}) |V_o| V_o \sin^3(\hat{\alpha}) +$$

$$\frac{1}{2} \rho Cd_{drogue} \left(\frac{\pi D_{drogue}^2}{4}\right) |V_o| V_o \tag{7b}$$

$$\widehat{F_Z} = F_N \sin(\hat{\alpha}) + F_T \cos(\hat{\alpha}) + F_B - F_W \tag{8a}$$

$$= \frac{1}{2} \rho Cd_N (D_{FO} L_{FO}) |V_o| V_o \cos^2(\hat{\alpha}) \sin(\hat{\alpha}) +$$

$$\frac{1}{2} \rho Cd_T (\pi D_{FO} L_{FO}) |V_o| V_o \sin^2(\hat{\alpha}) \cos(\hat{\alpha}) + \rho g (\gamma - 1) \left(\frac{\pi D_{FO}^2}{4} L_{FO}\right) \tag{8b}$$

If the cable is near taught, the constant slope angle can be approximated as $\hat{\alpha} \cong \cos^{-1} \frac{\widehat{\Delta z}}{L}$, and $\frac{\widehat{\Delta z}}{L}$ is found using Equation (6). Figure 31 shows how F_X from the OrcaFlex model compares to $\widehat{F_x}$ which was calculated using (7b). The dashed line is a one-to-one slope. They are nearly identical except for a few points when velocities were small. The R^2 is 1.0. This strong fit

means the curvature of the cable had little influence in modifying the force parallel to the flow. As shown earlier, the drogue dominated tension in the x-direction since the drogue provided significantly more drag than the cable itself. The largest drag occurred at the maximum velocity either with the largest drogue or the largest cable. Note that a 0.003 m cable was not tested with the largest drogue; the drogue diameter was only varied for the base case 0.001 m diameter cable.

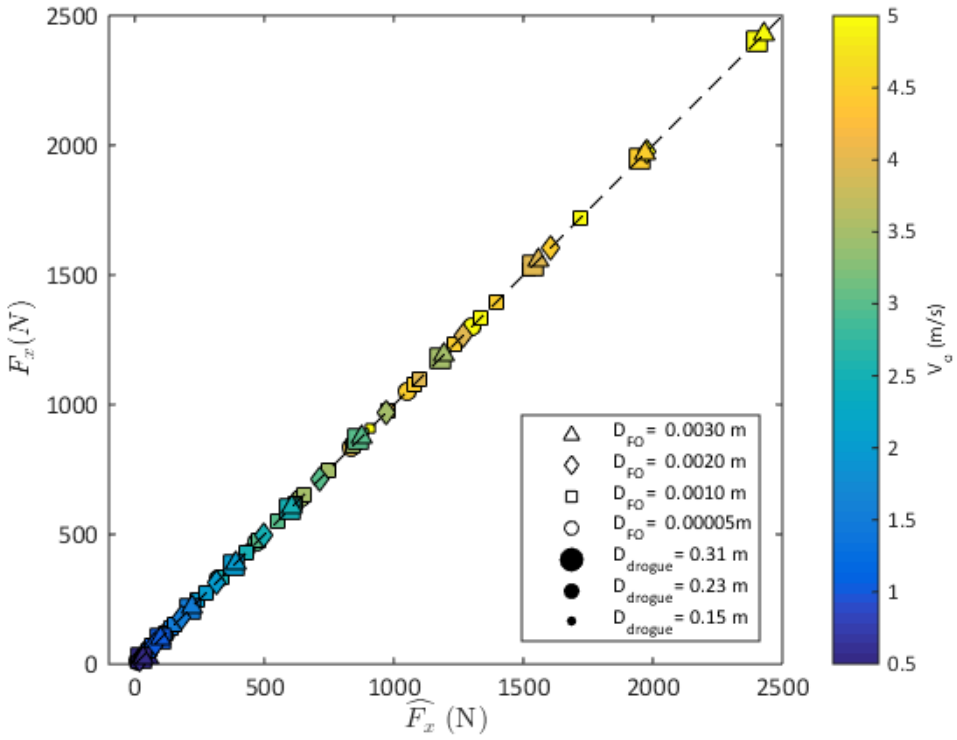

Figure 31. FOMC tension on the depressor in the x-direction, comparing the model result, F_X, to the calculated estimate, $\widehat{F}_x$, for all cases.

Forces in the z-direction were not as predictable. Figure 32 shows a comparison between the modeled F_Z and predicted $\widehat{F}_Z$ for all cases. When velocities were above 1.5 m/s, Equation (8b)

provided accurate predictions of the model. This is also the speed where the cable became nearly parallel to flow, removing all curvature in the line makes F_T solvable through analytics and F_N=0. When the cable diverged furthest from axial flow, namely where V_o < 1.5 m/s and $|\gamma$-1|>=0.10, the FOMC also experienced its greatest amount of curvature. Normal forces would therefore be less than those predicted using a straight cable assumption. But even after normal forces were removed, there was still divergence at low velocities suggesting that the tangential drag also reduces in a non-linear way with reductions in velocity. The author's attempts to parameterize this divergence were unsuccessful. It does appear sigmoidal with respect to velocity but no standard sigmoidal function applied to the tangential component of $\widehat{F_Z}$ improved the F_Z vs. $\widehat{F_Z}$ plot significantly enough to warrant its inclusion.

The curvature of the FOMC appears to play a significant role in predicting vertical forces. Understanding vertical forces are important for keeping the depressor at the prescribed depth. If the FOMC does have flexural strength, which was assumed to be zero in this study, higher velocities will be needed to reach axial flow. At low velocities, the magnitudes of F_Z, F_N and F_T will be less than predicted.

Even though predictions for F_Z are not accurate at low velocities, the parallel force F_X is still dominant and the combined force $\sqrt{\widehat{F_X}^2 + \widehat{F_Z}^2}$ provides an accurate prediction of the max tension in the cable, F, as shown in Figure 33.

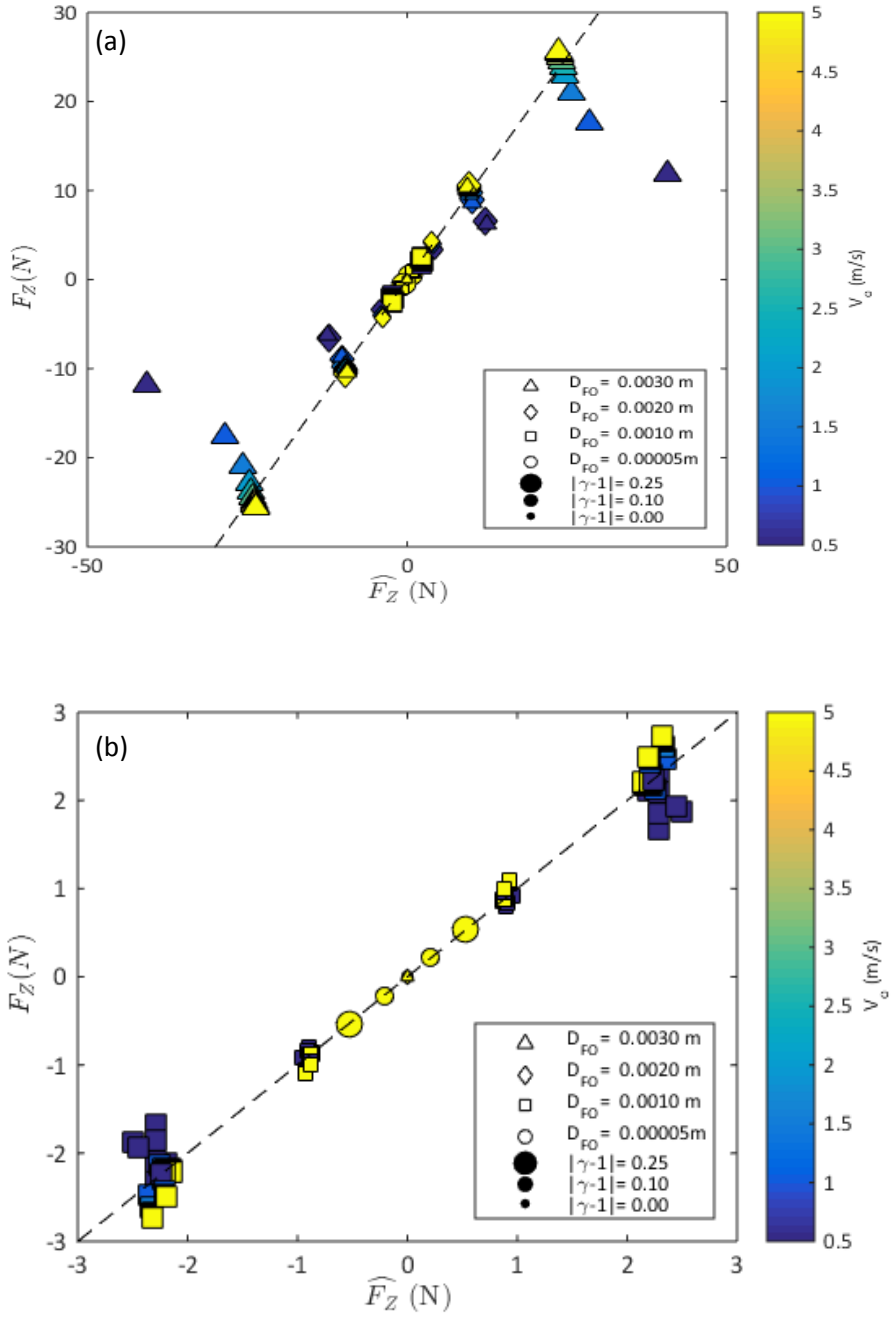

Figure 32. FOMC tension on the depressor in the z-direction, comparing the model result, F_Z, to the calculated estimate, $\widehat{F_Z}$. (a) all cases. (b) Zoomed into -3 N to 3 N.

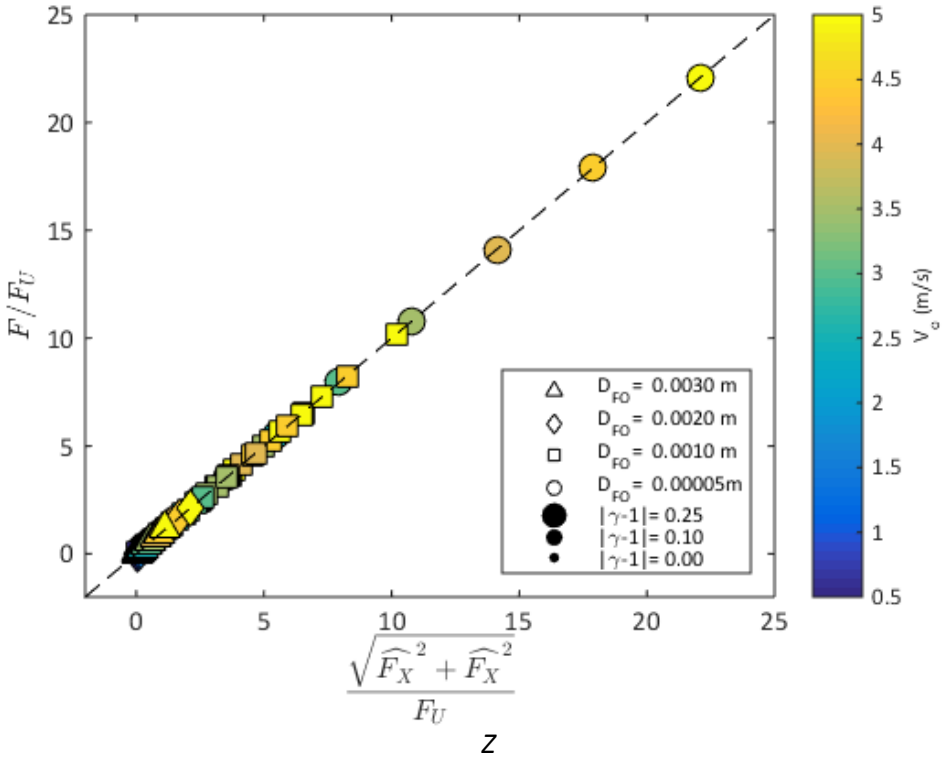

Figure 33. Maximum tension of the FOMC compared to the Pythagorean summation of $\widehat{F}_X$ and $\widehat{F}_Z$ for all cases.

3.5. Conclusions from Parametric Study

Part one of this study explored the parametric sensitivities of a towed fiber-optic micro cable. The model assumed that the FOMC is a non-extensible strength acting in water that has a constant density and temperature and that wave action does not alter the system. The following conclusions were demonstrated to be true for this 1,000 m cable.

1. A semi-analytical expression (Equation (6)) can be used to predict the rise of the drogue end above or below the horizontal and is a function of specific gravity, cable diameter, cable tangential drag, velocity, and drogue diameter. Further approximations of the analytical expression (Equations (7) and (8)) provide simplified predictions for the

maximum force components of the cable. All three equations work best at higher velocities when the cable is pulled straight.

2. The cable tension and excursion is insensitive to the tangential drag coefficient. The drogue provides far greater tension than the skin drag. Any changes that the skin drag coefficient might have are attenuated by the pull force at the end of the cable.
3. The most influential parameter on ΔZ, other than ship speed and specific gravity, is the cable diameter because of its exponential influence on buoyancy. Although the cable diameter also increases drag forces, it is insufficient to overcome the added buoyancy.
4. Slight changes in buoyancy (+/- 25%) can lead to a worst case vertical travel of +/- 260 m at speeds of 1 m/s (1 knot) or less. For shallow deployments, this may become close enough to the surface to be influenced by surface waves, or in deep deployments care must be taken to not strike the bottom.
5. Cable tension is primarily influenced by ship speed and drogue size.
6. When measured at the depressor end, increases in cable tension will cause the cable to rise until the strength member is taught. Once the strength member is nearly axial, increases in cable tension will reduce the curvature of the strength member so that the depressor sits slightly lower in the water.
7. Vertical lift on the depressor is minimal in all cases, and is mainly influenced by the buoyancy of the cable, and to a lesser extent, it is influenced by the tangential drag.
8. If this numerical experiment were to be performed with a physical model, this study suggests the following equipment and limits will be appropriate to analyze the cable:
    a. Depressor weight has little ability to influence the overall depth of the cable, so deploy the heaviest depressor the ship hoist and strength member is able to safely handle. A 0.25 te was the heaviest depressor used in this model. Drag reducing measures such as fairing the strength member, stream lining the depressor, or adding negative lift wings to the depressor may have more influence than adding additional mass.

b. A nine inch drogue is sufficient. It is important to get the precise force vs. speed charts for the selected drogue.
c. Ship speed should be kept below 2.0 m/s (4 knots) to ensure tension on the cable stays below F/F_U=1.0. The exact limiting speed depends on the size of the drogue and size of the cable.
d. A ½", 6x19 wire rope or larger is a sufficient size for the strength member.

4. Cable Deployed from ROV

4.1 Experiment Description

The physical experiment is a constantly moving target that has gone through multiple iterations of planning. On May 12, 2016, after much of the previously discussed analysis was completed, EXWC provided a new planned setup for the physical experiment they plan to conduct later in the summer of 2016. The schematic is shown in Figure 34. An ROV driven by a support vessel will deploy the FOMC from an attached winch. The opposite end of the FOMC will be attached to a suspended line anchored to the sea floor and held in place vertically by two buoys, one containing an acoustically triggered release mechanism to aid in recovery. The ROV will be self-powered traveling at up to 0.5 m/s. The winch is tension controlled, paying cable out when the tension is between 2 N to 67 N (½ lbs. to 15 lbs). If tension is below the limit, the ROV keeps traveling to increase the tension. If the tension is above the limit, then a brake is applied to prevent the cable from paying out too much, too quickly. After the cable reaches L_{FO}= 500 m, the ROV and cable will be left in place for a period up to 24 hours to check the cable resiliency. The ocean environment is expected to have waves no longer than 400 m so the cable and ROV should not experience any wave action. Undersea currents may be up to 20 cm/s in any direction.

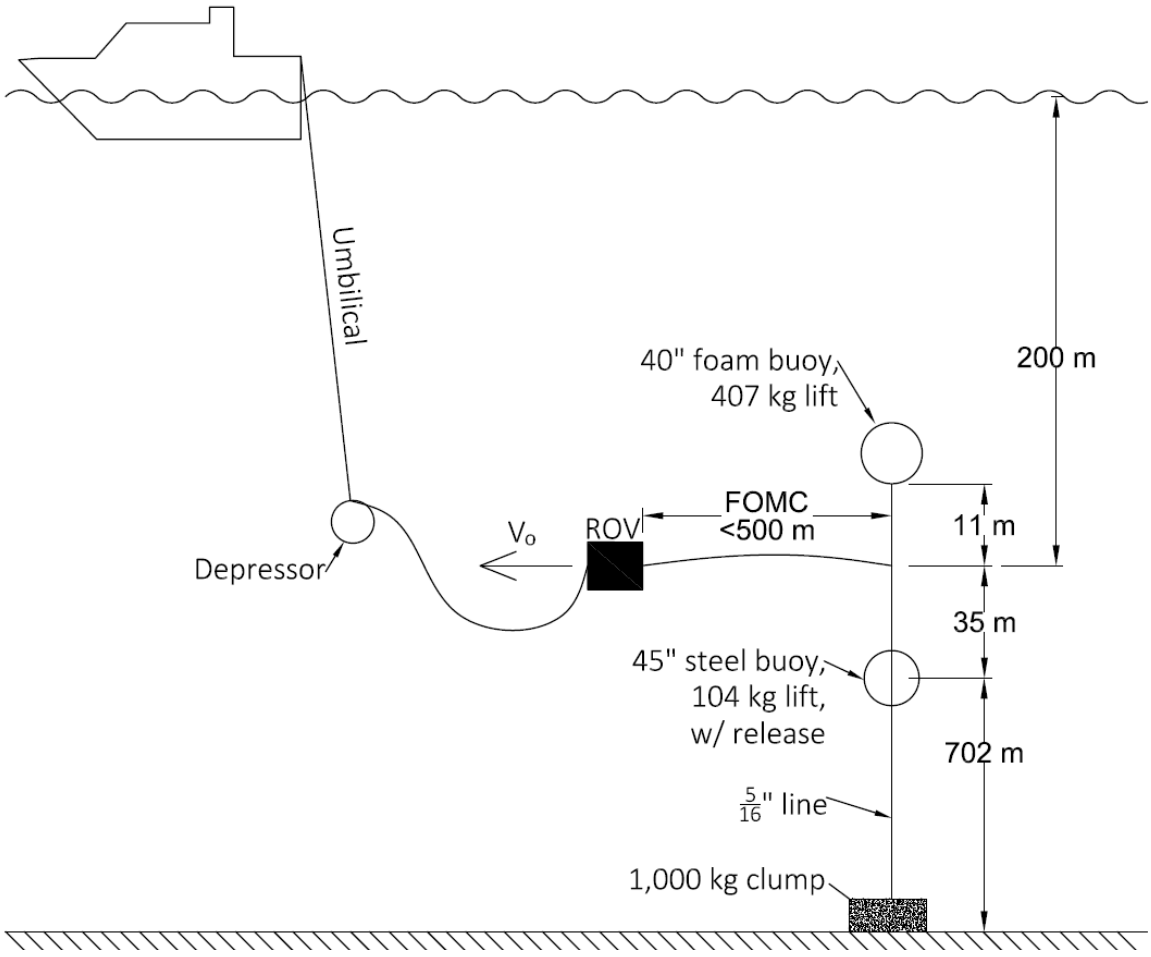

Figure 34. Schematic of the physical experiment deploying the FOMC from an ROV. Not to scale.

4.2 Discussion

It is important to predict the tensions on the cable in order to prevent excessive payout resulting in the cable entangling itself. Based on results from the parametric study, a few predictions can be made about this new setup. Cable diameter is expected to have the most influence on drag and elevation. If the current is acting parallel to the FOMC, then max tension can be assumed to be a combination of tangential drag and buoyancy:

$$F=\sqrt{(F_B-F_W)^2+\left(\frac{1}{2}\rho Cd_T\pi D_{FO}L_{FO}V_o^2\right)^2} \quad (9)$$

If the current is acting normal to the cable, then max tension can be found by:

$$F=\frac{1}{2}\sqrt{(F_B-F_W)^2+\left(\frac{1}{2}\rho Cd_N D_{FO}L_{FO}V_o^2\right)^2} \quad (10)$$

The ½ assumes that the tension is equally supported by both ends of the FOMC and the ROV only receives ½ the force. If 2 N is used as the release tension, than there is some V_{crit} where drag and buoyancy combine to exceed this value. Deploying the FOMC in currents above this amount would results in excessive payout. V_{crit} can be found using the following equations:

$$V_{crit,T}=\sqrt{\frac{2}{\rho Cd_T\pi D_{FO}L_{FO}}\sqrt{(2\ N)^2-(F_B-F_W)^2}} \quad (11)$$

$$V_{crit,N}=\sqrt{\frac{2}{\rho Cd_N D_{FO}L_{FO}}\sqrt{(2(2\ N))^2-(F_B-F_W)^2}} \quad (12)$$

The resulting critical currents are shown in Figure 35. All coefficients are carried over from the original study except that Cd_N is assumed to be a constant 0.3. Cable buoyancy does not provide a significant component of the overall tension and therefore does not affect the critical velocity. It appears that the 2 N (1/2 lbs.) peel tension is set too low if cross-flow currents of 20 cm/s are expected, unless the cable is only 0.0005 m thick. If currents are expected, it is best to operate the ROV in the direction of the current so that normal drag is minimized and the cable tension pulls on the riser rather than the ROV.

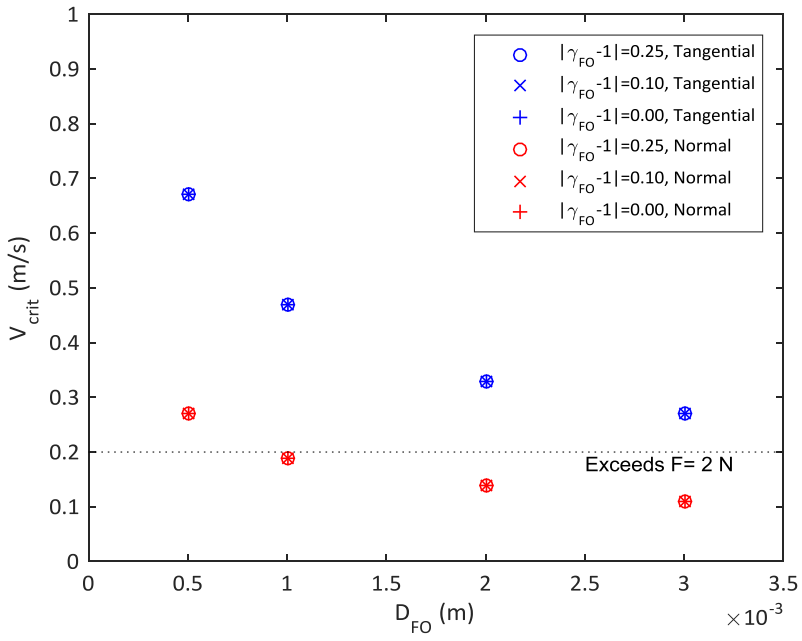

Figure 35. Critical current velocities in both normal and tangential flow to reach 2 N.

Using Equation (9), new peel tension settings are recommended in Table 6 based on cable diameter and using a maximum cross current of 30 cm/s.

Table 6. Recommended Peel Tensions

D	Peel	
(m)	(N)	(lbs)
0.0005	2	0.4
0.001	3	0.8
0.002	7	1.6
0.003	10	2.4

5. Summary and Future Work

This paper supports Phase 1 of a multi-year development study for DARPA's TUNA project. A parametric analysis was performed on a two-part cable deployment for a near-buoyant, fiber-optic micro cable with length-to-diameter ratios ranging between 3×10^5 to 2×10^6. This analysis demonstrated the sensitivity that the cable tension and elevation has to cable buoyancy and diameter, and how it is insensitive to the axial drag coefficient when attached to a drogue chute. The semi-analytical equations presented provide good predictions of the FEM results for tension in both x and z and the drogue excursion.

These results were applied where applicable to the latest version of the physical experiment that EXWC plans to conduct later this summer. The planned peel tension of ½ lbs is likely to result in excessive slack in the presence of 20 cm/s cross currents if the diameter exceeds 0.5 mm; a list of recommended peel tensions is provided for each cable diameter.

EXWC is planning to conduct their physical test in late-summer 2016. This corresponds to the timeframe when the author will transfer to his new unit located near EXWC headquarters at Naval Base Ventura County where he can provide additional on-site support if requested.

Acronyms Used

DARPA	Defense Advanced Research Projects Agency
EXWC	Naval Facilities Engineering Command, Engineering and Expeditionary Warfare Center
FEM	Finite Element Model
FOMC	Fiber-optic micro cable
LCP	Liquid Crystal Polymer
NAVFAC	Naval Facilities Engineering Command
TUNA	Tactical Undersea Network Architectures

Symbols Used

Roman Letters

A	drag area
Cd	drag coefficient
D	diameter
F	force
g	gravity
M	mass
L	length
T	temperature
V	velocity

Greek Letters

α	angle between flow velocity and the cable's normal vector
ε	roughness coefficient
γ	specific gravity
ρ	density

υ	kinematic viscocity

Subscripts

depressor	depressor weight
drogue	drogue chute
FO	fiber optic cable
N	normal
o	free flow
r	relative
T	tangential
x,y,z	direction relative the body or global system

References

Antunes, P., Domingues, F., Granada, M., & Andre, P. (2012). Mechanical Properties of Optical fibers. *Selected Topics on Optical Fiber Technology*. (D. M. Yasin, Ed.) InTech. Retrieved from http://www.intechopen.com/books/selected-topics-on-optical-fiber-technology/mechanicalproperties-

Choc, Y.-I., & Casarella, M. (1971). Hydrodynamic Resistance of Towed Cables. *Journal of Hydronautics, 5*(4), 126-131.

Commander, Naval Sea Systems Command. (2000). *U.S. Navy Salvor's Handbook.* U.S. Navy.

ESDU 80025. (1986). *Mean forces, pressures and flow field velocities for circular cylindrical structures: single cylinder with two-dimensional flow.* London: Engineering Sciences Data Unit.

Hinz, E. R. (1987). *Understanding Sea Anchors and Drogues.* Centreville, Maryland: Cornell Maritime Press.

Holler, R. (1984). *Drag measurements of long cables in the ocean, No. NADC-84086-30.* Naval Air Systems Command, Warminster, PA.

Kaneko, I., Takatsuki, Y., Kamiya, H., & Kawae, S. (1998). Water property and current distributions along the WHP-P9 section (137ø-142øE) in the western North Pacific. *J. of Geophysical Research: Oceans, 103*(C6), 12959-12984. Retrieved from 10.1029/97JC03761

Karnoski, S. (1991). *A model for the tangential component of hydrodynamic drag on small diameter cables based on labroratory tests, T.M. 43PI-91-02.* Naval Civil Engineering Laboratory, Port Hueneme, CA.

Kheiri, M., Paidoussis, M., & Amabili, M. (2013). A nonlinear model for a towed flexible cylinder. *Journal of Sound and Vibration, 332*, 1789-1806.

Leonard, J., & Karnoski, S. (1990). Simulation of tenstion controlled cable deployment. *Applied Ocean Research, 12*(1), 34-42.

Linden Photonics, Inc. (2006). *Liquid Crystal Polymer MEMS Packaging*. Retrieved June 08, 2016, from Linden Photonics, Inc.- Technology: http://www.lindenphotonics.com/technology.php

Linden Photonics, Inc. (2014). STFOC Optical Cable Non-Kink Crush Proof Brochure. Westford, Massachusetts. Retrieved May 2016, from http://www.lindenphotonics.com/

Lopes, J.-L., Paidoussis, M., & Semler, C. (2002). Linear and nonlinear dynamics of cantilevered cylinders in axial flow. Part 2: The equations of motion. *Journal of Fluids and Structures, 16*(6), 715-737.

Mitsubishi Rayon Co., Ltd. (n.d.). *Eska Polymer Optical Fiber.* Optical Fiber Department, Tokyo. Retrieved 04 23, 2016, from www.pofeska.com

Morison, J., O'brien, M., Johnson, J., & Schaaf, S. (1950). The Force Exerted by Surface Waves on Piles. *Petroleum Transactions, AIME, 189*.

Morrison, F. (2013). *An Introduction to Fluid Mechanics.* New York: Cambridge University Press.

Nayar, K., Sharqawy, M., Banchik, L., & Lienhard V, J. (2016). Thermophysical properties of seawater: A review and new correlations that include pressure dependence. *Desalination, 390*, 1-24. Retrieved from 10.1016/j.desal.2016.02.024

Orcina. (2009). *OrcaFlex user manual.* Ulverston, UK: Orcina.

Paidoussis, M. (1966). Dynamics of flexible slender cylinders in axial flow. part 1: Theory. *Journal of Fluid Dynamics, 26*, 717-736.

Paidoussis, M. (1973). Dynamics of cylindrical structures subjected to axial flow. *Journal of Sound and Vibrations, 204*, 835-840.

Paidoussis, M., Grinevich, E., Adamovic, D., & Semler, C. (2002). Linear and nonlinear dynamics of contilevered cylinders in axial flow. part 1: Physical dynamics. *Journal of Fluids and Structures, 16*(6), 691-713.

Reid, R., & Wilson, B. (1962). Boundary flow along a circular cylinder. *National Engineering Science Company, T.R. 204-4*.

Rispin, P. (1977). *Drag of the thin line towed array.* David W. Taylor Naval Ship Research and Development Center, Ship Performance Department, Bethesda, MD.

Sarpkaya, T. (2010). *Wave Forces on Offshore Structures.* New York: Cambridge University Press.

Semler, C., Lopes, J.-L., Augu, N., & Paidoussis, M. (2002). Linear and nonlinear dynamics of cantilevered cylinders in axial flow. part 3: Nonlinear dynamics. *Journal of Fluids and Structures, 16*(6), 739-759.

Sharqawy, M., Lienhard V, J., & Zubair, S. (2010, Apr). Thermophysical properties of seawater: A review of existing correlations and data. *Desalination and Water Treatment, 16*, 354-380.

Triantafyllou, G., & Chryssostomidis, , C. (1985). Stability of a string in axial flow. *Journal of Energy Resources Technology, 107*(4), 421-425.

Versprille, A. (2016, February). Emergency Military Network to Go Under Sea. *National Defense*. Retrieved from

http://www.nationaldefensemagazine.org/archive/2016/February/Pages/EmergencyMilitaryNetworktoGoUnderSea.aspx?PF=1

White, F. (1972). An Analysis of Axisymmetrc Turbulent Flow Past a Long Cylinder. *Journal of Basic Engineering* , 200-204.

Zhou, X.-J., Wei, W., & Xiang, W. (2008). Research on sinkage of submarine fiber optic micro-cable deployed at high speed. *Journal of Naval University of Engineering, 20*(5), 46-50.